KERNFORSCHUNGSZENTRUM

KARLSRUHE

Juni 1968

KFK 811
EUR 3970 e

Institut für Neutronenphysik und Reaktortechnik
Institut für Angewandte Reaktorphysik

Uranium Reaction Rate Measurements in the Steam-Cooled Fast Reactor SNEAK, Assembly 3A-2

R. Böhme, H. Seufert

GESELLSCHAFT FUR KERNFORSCHUNG M. B. H.

KARLSRUHE

KERNFORSCHUNGSZENTRUM KARLSRUHE

Juni 1968

KFK 811
EUR 3970e

Institut für Neutronenphysik und Reaktortechnik

Institut für Angewandte Reaktorphysik

Uranium Reaction Rate Measurements in the Steam-Cooled Fast Reactor SNEAK, Assembly 3A-2 *

by

R. Böhme and H. Seufert

* Work performed within the association in the field of fast reactors between the European Atomic Energy Community and Gesellschaft für Kernforschung m.b.H., Karlsruhe.

Abstract

Uranium reaction rate traverses as well as their fine structure have been measured at the Karlsruhe Fast Zero Power Reactor SNEAK assembly 3A-2. For this purpose uranium metal foils were irradiated in the reactor. The γ-x-ray coincidence technique was applied to determine the relative capture rates in ^{238}U. To get absolute rates by this method the counting equipment was calibrated by a ^{243}Am source [1]. The relative fission rates were obtained by integral counting of the fission product γ-activity above 660 keV γ-energy. These rates were linked to an absolute parallel plate fission chamber experiment. The experimental rate ratios were compared with calculated ones. The traverse measurements indicate a strong dependency of the axial "buckling" (relative second derivative of the rates) on energy. The calculations with the Karlsruhe SNEAK-set yield these bucklings in the average 5% higher than measured. The calculated fission rate ratio $\sigma_f^{28}/\sigma_f^{25}$ is 13 to 20% lower than the measured one depending on the heterogeneity of the core, but the capture to fission rate ratio agrees better with the measurement. An additional k-infinity experiment would point more directly to the source of this inconsistency. The intitial breeding ratio IBR of a slab reactor is defined by:

$$IBR_z = \frac{\int_{z\text{-axis}} \varrho^{28} R_c^{28}(z)\, dz}{\int_{z\text{-axis}} \varrho^{25} R_f^{25}(z)\, dz} \cdot \frac{1}{1 + \dfrac{\int_{z\text{-axis}} \varrho^{25} R_c^{25}(z)\, dz}{\int_{z\text{-axis}} \varrho^{25} R_f^{25}(z)\, dz}} .$$

Because the capture integral of ^{235}U is experimentally not accessible only the first quotient could be measured and compared with theory but, of course, for a finite cylindrical reactor. Due to error compensation the measured and calculated quotients agree within a 4% error limit. A comparison of spectral indices measured by foils in a cavity of 5 x 5 x 20 cm^3 volume and in the original cell show a discrepancy of 29% for $\sigma_c^{28}/\sigma_f^{25}$ and - 8% for $\sigma_f^{28}/\sigma_f^{25}$. Therefore, parallel plate chamber experiments are difficult to interpret. These results refer to the normal unit cell of the SNEAK assembly.

1. Introduction

This work is part of the reactor physics investigations performed at Karlsruhe in the field of hydrogen containing assemblies. Because the power density and the breeding ratio of such systems are of special interest in reactor design it is necessary to measure these quantities absolutely and to compare them with calculations.

The measurements were carried out on SNEAK assembly 3A-2. This is a uranium metal fueled reactor (20% enrichment) with an average hydrogen content of $1.8 \cdot 10^{21}$ atoms/cm^3 in the core region. The blanket of high density consists mainly of depleted uranium metal. A complete description of this reactor is given in [2].

This paper deals with the experimental determination of

(a) axial reaction rate traverses,
(b) fine structure of reaction rates.

From these measurements we obtained characteristic quantities like buckling and breeding ratio. In addition, reactor calculations in diffusion approximation and cell calculations with collision probability methods [3] were carried out and compared with the experimental results.

An attempt is made to explain rather great differences between measured and calculated reaction rate distributions within a cell and along the reactor axis. Assuming that the fission cross sections of ^{235}U and ^{238}U are correct, one has to assume that the actual spectrum in the fuel region is harder than the calculated one. This would agree with the difference in the theoretical and measured multiplication constant k_{eff}. In this sense reaction rate distributions are a helpful tool for checking cross section sets and calculational methods.

2. Experimental Methods and Calibration Techniques

Fission and capture rates of uranium were measured by irradiation of pure uranium metal foils of different enrichment. The ^{235}U content of the depleted foils was 0.44 and of the enriched foils 20.04 weight percent. The foils had a diameter of 2.54 cm, their weight was in the range of 0.9 grams and within one reaction rate distribution experiment varied in the range $\pm$ 1%. For irradiation, two foils of different enrichment were enveloped in 10 µm thick aluminium foils. The foils were irradiated in the SNEAK reactor for three hours at a reactor power of about 50 watts. After a cooling period of around three days the γ-activity of the foils was counted in the 106 keV range applying the γ-x-ray coincidence method, above 660 keV single channel counting was used. Counting was accomplished by an automatically operated sample changer [4] and electronic apparatus. A block diagram of the electronic circuits is shown in Fig.1. The special feature of this equipment is the automatically controlled pulse height in each channel. This is performed by two digital units stabilizing on the 106 keV capture peak of the depleted foil and on the pronounced peak around 100 keV of the enriched foil, respectively. This stabilization is essential since the pulse height depends strongly on the activity of the foil [5].

To exclude the complex decay law of the fission product activity all foils of one irradiation were repetively counted in a forward and backward cycle. The measuring time for each foil within one cycle was 100 sec. Each counting interval was followed by a seven seconds foil changing and an additional seven seconds stabilization time. Normally, the total counting period was 2 to 3 days.

The γ-x-ray coincidence apparatus was absolutely calibrated by means of a ^{243}Am source [1], the decay rate of which is absolutely known with an accuracy of 0.5 %. It is assumed that the γ-activity above 660 keV is a measure of the fissions which occured in each foil. The activities z_d and z_e of the depleted and enriched foils, irradiated at the same position x, can be used to determine the fission rates per gram, R_f, of ^{235}U and ^{238}U:

$$R_f^{25}(x) \cdot f^{25}(t) = \frac{m_d^{28} z_e(t) - m_e^{28} z_d(t)}{m_e^{25} m_d^{28} - m_d^{25} m_e^{28}}$$

$$R_f^{28}(x) \cdot f^{28}(t) = \frac{m_e^{25} z_d(t) - m_d^{25} z_e(t)}{m_e^{25} m_d^{28} - m_d^{25} m_e^{28}} \quad , \qquad (1)$$

where $m_{d(e)}^{28}$, $m_{d(e)}^{25}$ are the masses of ^{238}U, ^{235}U in the depleted (enriched) foil.

The factors f include the decay law of the fission products and the counter sensitivity.

If the fission rate is absolutely known at a certain position in the reactor the factors f can be determined from a pair of foils irradiated at this position. Such a position is given inside an absolutely calibrated parallel plate fission chamber. Therefore, one pair of foils was irradiated in each run inside this fission chamber, which was located 22 cm off the core center. The influence of resonance selfshielding in the enriched foil irradiated in the parallel plate chamber is negligible. This will be discussed in 7.1.

3. Statistical and Systematic Error Analysis

By repeated measurement of each activated foil a statistical accuracy better than 0.3 % could be achieved both in coincidence and high energy γ-counting. Because of this high statistical accuracy no error bars are indicated in the figures. An estimation of the errors in fission rates due to statistics and uncertainties in isotopic composition yields 0.1 % in R_f^{25} and 0.5 % in R_f^{28}. This is simply obtained by application of the error propagation law to formula (1). Nevertheless, discrepancies in the order of 2 percent were found, for instance, by measuring two pairs of foils in comparable positions. It is assumed that this error could arise from the following sources:

A. Error Estimation for Capture Rates

1. The capture rate was determined by assuming a half-life of ^{239}Np of 2.35 d. This half-life is quoted in literature, but our measurements yielded half-lives between 2.31 and 2.40 days in extreme cases. Therefore, a reasonable error of 1% is assumed in the half-life. Since the measurements were carried out usually one or two half-lifes after irradiation the measured capture rate may be wrong by 1.5 %. The reason for measuring different half-lifes is probably caused by insufficient electronic stability of the apparatus. This effect is discussed in more detail below.

2. Although a very precise positioning of samples between the detectors is achieved, small errors in the counting rates cannot be excluded. A relative error of 0.5 % may be due to this effect.

B. Error Estimation for Fission Rates

1. All fission rates were related to fission rates measured in foils irradiated inside absolutely calibrated parallel plate fission chambers. The calibration of the fission chambers is given with an accuracy of 2% in each rate and 3% in the fission rate ratio.

2. Besides this calibration error of the parallel plate chambers an inaccurate determination of irradiation dose must be accounted for. This does not affect the fission rate ratio but the capture to fission rate ratio. This error is assumed to be in the order of 1%.

3. As described in paragraph 2 the γ-spectrum of each foil was stabilized digitally. This stabilization started 7 sec before each counting interval of 100 sec. Nevertheless, the counting rates in the channels of the forward and backward cycle deviated up to 0.5 % depending on the activity of the foil counted previously. This effect can be explained by the strong dependence of the multiplier amplification on the counting rate [5]. Since the relaxation time of the multiplier is of the order of minutes the 7 sec stabilization before each counting is not sufficient to produce steady state conditions. Therefore, it is proposed to use depleted and enriched foils of different thickness but approximately equal activity in future experiments.

It should be remarked that stabilizing is done for both foils of different enrichment on the γ-peak around 100 keV, although the capture and ^{235}U γ-peaks deviate by 6 keV. Therefore, the energy threshold for the depleted and enriched foils are not identical. But this results in no additional error, if the fission rate ratio and the capture-to-fission rate ratio do not vary extremely for all pairs of foils. This can be deduced from formula (1) in which only the factors f include the energy threshold. The total errors for R_f^{25}, R_f^{28}, R_c^{28}, and the rate ratios are given in Tab.1.

4. Description of Reactor and Cell Structure

A vertical cross section of the SNEAK reactor, assembly 3A-2, is shown in Fig.2. The cylindrical reactor consists of two core regions and one blanket region. The average compositions of the central zone and the blanket are given in Tab.2. The average composition of core zone 2 deviates from core zone one by less than 1% for each material except for hydrogen ($17.45 \cdot 10^{20}/cm^3$). All experiments were carried out along the central z-axis.

The core region around the central axis is made up of equal cells each containing four platelets of different material as shown in Fig.3. Instead of the aluminium 25% platelets usually used in SNEAK, special platelets were fabricated which are better adapted for the calculation of reaction rates in a unit cell. The geometry of these platelets is also given in Fig.3. The compositions of the platelets are summarized in Tab.3.

In Tab.3 the stainless steel (SS) of the surrounding subassembly wall is added uniformly to the platelets. The edge length of the platelets was assumed to be 54.4 mm. This length is equal to the period of the core matrix.

The reaction rate measurements were also carried out in bunched cells. Bunching was accomplished by multiplying the thickness of each platelet by a factor of two or four. To measure the reaction rate distribution within a 20% enriched uranium platelet a modification was necessary. The arrangement of the foils in this platelet is shown in Fig.4. In all other cases the uranium foils were simply inserted between the platelets. To keep the additional uranium content in the cell introduced by the foils as low as possible the foils were usually distributed over two adjacent cells.

5. Measurement of Uranium Reaction Rate Traverses and Evaluation of Bucklings

It was assumed that the axial distribution of reaction rates is modulated by a fine structure due to the heterogeneous arrangement of the cell. Therefore, together with the traverse measurement the reaction rate distributions in two unit cells were measured. One of these cells was positioned near the midplane of the core, the other 35 cm off the midplane near the core blanket boundary. In spite of the strong gradient affecting the distribution inside the second cell the spatial variation of the spectral indices $\sigma_c^{28}/\sigma_f^{25}$ and $\sigma_f^{28}/\sigma_f^{25}$ is almost the same in both cells (see Fig.13). Therefore, the assumption that fine and coarse structure are separable seems to be justified. Due to the difference in the bucklings of the three measured reaction rates the absolute values of reaction rate ratios are not identical (see below). Therefore, the bucklings were determined from foils placed in corresponding cell positions. But the central values of the average reaction rate ratios in the uranium platelets were obtained after correction for this fine structure.

The axial reaction rate distributions corrected for cell fine structure are shown in Fig.5. To these measured points a cosine fit was attempted between $z = \pm 34$ cm core height. The fitted cosines with the measured data are sketched in Fig.6. The bucklings obtained in this way are:

$$B^2\,(R_f^{25}) = (8.025 \pm 0.032) \cdot 10^{-4}\ \mathrm{cm}^{-2}$$

$$B^2\,(R_f^{28}) = (8.922 \pm 0.028) \cdot 10^{-4}\ \mathrm{cm}^{-2}$$

$$B^2\,(R_c^{28}) = (7.868 \pm 0.024) \cdot 10^{-4}\ \mathrm{cm}^{-2}\ .$$

A rigorous error estimation is carried out in Appendix A. The quoted errors are the estimated variances of the cos-fit. It can be shown [+] that the t-test is applicable to the parameters of a least-square fit. In our case, the number of degrees of freedom, which is the number of measured points minus the number of fitted parameters, is eight. Therefore, the quoted errors in B^2 have to be multiplied by 2.30 if a 95% confidence level is required.

6. Reaction Rate Distributions in Normal and Bunched Cells

A series of heterogeneity experiments was carried out in SNEAK 3A-2. The cell thickness of the unit cells in a large central core region was increased by a factor of two (λ = 2.52 cm) and four (λ = 5.03 cm). In a further step the polyethylene content of the cell was increased by a factor of two. In this case the cells had four-fold thickness (λ = 5.03 cm). The reactivity effect connected with this bunching was measured. Since this integral measurement gives little information about the neutron physics involved the uranium reaction rate distribution in these different cells are of special interest (see Ref. [2]). The distributions of R_c^{28}, R_f^{25}, and R_f^{28} in the four types of cells are shown in Figures 7 to 10. Of main interest are the uranium reaction distributions in the fuel platelets. Integration of these reaction rate distributions over the uranium platelets give the true reaction rates. It is assumed that the stainless steel walls separating the fuel platelets in the radial reactor axis do not disturb the radial distribution of reaction rates. This assumption was checked by measuring the radial reaction rate distribution with foils of 10 cm diameter across the platelets. Common to all figures is a maximum of R_f^{28} and minima of R_f^{25} and R_c^{28} in the center of the uranium platelets. The multiplication of neutrons is mainly responsible for the peaking of R_f^{28}. The depression of R_f^{25} and R_c^{28} rates are typical resonance selfshielding effects. The strong selfshielding of the ^{238}U resonances is responsible for the steep gradient of R_c^{28} near the platelet surface. Therefore, any positioning uncertainties produce large errors in the R_c^{28}-values. The space-dependent spectral indices $\sigma_c^{28}/\sigma_f^{25}$ to $\sigma_f^{28}/\sigma_f^{25}$ of the different states of bunching are shown in Figures 11 to 14. In these figures the space coordinates were normalized to equal cell pitch. In this representation the spectral shift due to the degree of bunching is pronounced.

To obtain average reaction rates the distributions were integrated over the thickness of the uranium platelets. The reaction rates obtained by this procedure were used to normalize the measured traverses, because they were determined from foils positioned in aluminium platelets.

It should be noted that the spectral indices measured with parallel plate chambers in a cavity and with foils attached to the fuel platelets yield rather different values. The central ratio $\sigma_f^{28}/\sigma_f^{25}$ in the normal cell is $3.38 \cdot 10^{-2}$ measured by foils compared to $3.13 \cdot 10^{-2}$ determined with the chambers. The ratio $\sigma_c^{28}/\sigma_f^{25}$ measured in a chamber was 0.168 as compared with the actual ratio of 0.130 determined for the surrounding fuel. Both effects indicate that the spectrum in the cavity is similar to that in the structual material. Therefore, the true reaction rate ratios should be determined by foils which are part of the fuel itself.

7. Evaluation of Space Integrated Capture and Fission Rates

The normalization of reaction traverses as described in paragraph 5 allows the evaluation of the integrals of capture and fission rates along the z-axis of the cylindrical reactor SNEAK 3A-2. These integrals enter in the formula for the initial breeding ratio of an infinite slab reactor.

$$IBR_z = \frac{\int_{z\text{-axis}} \varrho^{28} R_c^{28}(z)\, dz}{\int_{z\text{-axis}} \varrho^{25} R_f^{25}(z)\, dz} \cdot \frac{1}{1 + \dfrac{\int_{z\text{-axis}} \varrho^{25} R_c^{25}(z)\, dz}{\int_{z\text{-axis}} \varrho^{25} R_f^{25}(z)\, dz}} \qquad (2)$$

It should be mentioned that only the first quotient is experimentally accessible in zero power reactors. Integration of the curves of Fig.5 yields with the proper correction factor and multiplied with the corresponding material densities ϱ :

$\varrho^{28} \int R_c^{28}(z)\, dz$ core	$\varrho^{28} \int R_c^{28}(z)\, dz$ blanket	$\varrho^{25} \int R_f^{25}(z)\, dz$ core	$\varrho^{25} \int R_f^{25}(z)\, dz$ blanket
$(5.23 \pm 0.10) \cdot 10^8$ capt./sec cm^2	$(2.56 \pm 0.06) \cdot 10^8$ capt./sec cm^2	$(10.10 \pm 0.23) \cdot 10^8$ fiss./sec cm^2	$(7.90 \pm 0.20) \cdot 10^6$ fiss./sec cm^2

This yields for

$$(1 + \overline{\alpha^{25}})\ IBR_z = 0.77 \pm 0.03 ,$$

where $\overline{\alpha^{25}}$ is defined by Eq.(2). The error estimation is based on systematical errors quoted in Tab.1 and the propagation of statistical errors dealt with in Appendix B.

8. Comparison of Experiments with Theory

To compare experimental with theoretical results two types of calculations were carried out.

A. Diffusion calculations in slab geometry, where the separated radial coordinate was taken into account by adding a DB_r^2 correction to the removal cross section. For these calculations, three 26-group cross section sets were available at Karlsruhe:

   1. The Russian cross section set ABN [6],
   2. the SNEAK-set compiled at Karlsruhe [7],
   3. the PMB-set which takes into account recent Karlsruhe cross section measurements [8].

   Most calculations were carried out for homogeneous core and blanket compositions. But in a few calculations with the SNEAK-set, corrections to the effective cross sections due to heterogeneity of the core were taken into account. Since these corrections by means of the ZERA program (see 8B) are obtained for the macroscopic cross section only, the rates were also calculated by multiplying the "heterogeneous" fluxes with "homogeneous" effective microscopic cross sections. The radial bucklings used in the slab calculations were obtained from a calculation of an infinite cylindrical reactor. All computer codes are part of the Karlsruhe program system NUSYS [7].

B. The reaction rate distributions within a cell for different degrees of bunching were calculated with the collision probability program ZERA [3]. In these calculations the SNEAK-set was applied only. Since this program requires the calculation of an infinite plane lattice, a DB^2 correction was applied which renders the lattice critical. The ZERA program assumes a flat source distribution within a uranium subregion; the thickness of a uranium platelet was, therefore, divided in up to nine subregions.

8.1 Central Reaction Rate Ratios

In Tab.4 the measured and calculated central reaction rate ratios are given for equal numbers of atoms. The experimental rate ratios for bunched cells are plotted together with ZERA calculated values in Fig.15. This figure also shows results for the SNEAK 3A-3 assembly which had twice the hydrogen density of SNEAK 3A-2. The most remarkable discrepancy of more than 10% between theory and experiment exists for the $\sigma_f^{28}/\sigma_f^{25}$ ratio. The theoretical $\sigma_c^{28}/\sigma_f^{25}$ ratio falls slightly out of the experimental limits of error only in the case of the normal cell. The variation of $\sigma_f^{28}/\sigma_f^{25}$ with increasing degree of bunching is much more pronounced than in the SNEAK calculation. In order to determine the sources of these discrepancies fine structure measurements are compared with rate calculations in Figures 16 and 17. In these drawings the calculations are arbitrarily normalized to the measured fission rate of ^{235}U. The spatial variations of the R_f^{28} and R_c^{25} rates are accurately calculated, but the depression of the R_f^{25} rate is underestimated in the fuel platelet in both cases of different hydrogen densities. The net distribution of the ^{235}U-fission rate is the sum of fast neutron fissions which are distributed like the ^{238}U-fissions and resonance neutron fissions distributed similar to the capture rate of ^{238}U. Because of this, the effect must be due to an underestimation of slow neutron fissions. Three explanations are possible:

A. The neutron spectrum in the fuel platelet is too hard,

B. the effective cross sections in the resonance region are too low,

C. the ZERA-code calculations may be insufficient in the low energy region.

Since the theoretical ratio $\sigma_f^{28}/\sigma_f^{25}$ is much smaller than the experimental one, it seems justified to rule out assumption A. If one traces back the creation of the SNEAK set from the ABN set [7] it could be assumed that the reduction of effective ^{235}U-fission cross sections (due to White's measurements) was too strong. The same effect was already indicated in measurements reported in [9] Fig.15. The spatial variation of the ^{235}U-fission rate was in between the calculations with the SNEAK and ABN set. From Ref. [7] it can also be deduced that the discrepancy in $\sigma_f^{28}/\sigma_f^{25}$ cannot be explained by erroneous ^{235}U fission cross sections only, since this discrepancy exists also for the ABN set. Therefore, one has to consider other effects which could be responsible for the much harder experimental spectrum. Similar discrepancies between experimental $\sigma_f^{28}/\sigma_f^{25}$ and calculated ratios were already reported in [10].

From the results obtained for different hydrogen densities in the double bunched case the conclusion can be drawn that the spectral effects from hydrogen are properly accounted for.

In this context a note to the calibration technique should be added: The fissionable layer of the parallel plate chamber and the enriched foil irradiated inside this chamber have different thickness, and, therefore, different neutron resonance selfshielding. In order to justify the calibration technique applied, the maximum uncertainty due to this effect was estimated from the series of bunching experiments. In Fig.18 the ratio of fission rates near the boundary and the midplane of the platelet are shown. From the extrapolation of these curves to the foil thickness 0.08 mm it can be concluded that the selfshielding effect amounts to less than 0.1 %.

8.2 Reaction Rate Traverses

Reaction rate traverses were measured for the normal cell structure only. In Fig.19 the ratios of calculated to measured reaction rates are shown without any normalization. Firstly, the core region is considered. The reason for the non-identical central ratios were already discussed in 8.1. Besides this, it is clearly visible that the calculated rates in the outer core region are too low. This effect is more pronounced for the SNEAK set calculations. From the comparison of cosine functions and measured reaction rates (see Fig.6) it seems justified to introduce a buckling for each measured reaction rate traverse. Bucklings B^2 are defined as the square of the half period of a cosine distribution fitted to the measured rates between $\pm$ 34 cm in the core region, because this region is not effected by the core blanket boundary. In Tab.5 the experimental bucklings are compared with theoretical values obtained by equivalent fitting procedure within $\pm$ 34 cm.

The bucklings defined in this way are rather artificial because their values depend slightly on the core region used for fitting.

All calculated bucklings are greater than the measured ones. This does not allow the conclusion that the leakage in general is higher in all calculations, since B^2 is equally affected by the diffusion constant and all other macroscopic cross sections. To get more experimental information a $k_\infty = 1$ experiment seems to be necessary.

8.3 The Core-Blanket Transition

It should be remarked that the calculated reaction rates approaching the boundary from the core and the blanket regions differ by more than 10% in the ^{238}U-capture rate, but by less than 2% in the ^{235}U-fission rate due to different space independent selfshielding factors in the core and blanket region. From Fig.19 it can be deduced that beyond $\pm$ 5 cm from the core blanket boundary such effects are of no importance. Comparing the Fig.19A and B no common trend in the reaction rate distributions in the blanket can be observed. This could be caused by the space independent but different weighting spectra in the SNEAK and ABN sets used for the calculation of the effective cross section sets. The smooth curves drawn through the points are extended only to the middle of the blanket, because the experimental errors increase rapidly towards the outer blanket boundary. This is caused by the steep decrease of reaction rates (see Fig.5) in the blanket. The reaction rate ratios shown in Fig.20 agree better with SNEAK set calculations in spite of the large errors in the rate distribution. This indicates again that the weighting procedure to obtain transport cross sections is unsatisfactory.

8.4 Reaction Rate Integrals

Because of the importance of space integrated rates their experimental and theoretical values are compared in Tab.6.

In Tab.6 the quotients theory-to-experiment are normalized to 1.000 for the integral fission rate in the core. With such a normalization most experimental data, with the exception of the capture rate in the core, agree with theory within the limits of error.

9. Summary

The cross section sets and calculational methods currently used at Karlsruhe do not allow a prediction of all measured quantities correctly. From the investigations reported in this paper the following agreements and disagreements can be found:

1. The k_{eff} values calculated with the SNEAK set disagree by 1.5 % in accordance with the discrepancies in theoretical and experimental reaction rate ratios.

2. The measured central $\sigma_c^{28}/\sigma_f^{25}$ ratio is 5% $\pm$ 3% lower than the calculation with the SNEAK set but 6% $\pm$ 3% higher than the ABN result. All calculated central fission ratios are at least 13% $\pm$ 3% lower than the measured values.

3. The variation in the central fission ratio with the degree of bunching is not satisfactorily described by theory.

4. The reaction rate distributions in the fuel platelets themselves agree rather well for ^{238}U-capture and ^{238}U-fission but not for ^{235}U-fission.

5. All reaction rates in the outer core region are underpredicted by diffusion theory with respect to their central values.

6. Although the rate distributions in the uranium blanket are not accurately calculated the reaction rate ratios are fairly well predicted by SNEAK set calculations.

7. The influence of a doubling of the hydrogen density in the core region on the reaction rates is satisfactorily described by SNEAK set calculations.

Acknowledgements

We are very indepted to Mr. D. Kuhn for carrying out the absolute calibration of the fission rates by means of parallel plate chambers. We are also very grateful to Dr. D. Wintzer for providing us with ZERA calculations and helpful discussions.

Appendix

A. Error Analysis of Fitted cos-Bucklings; Calculation of the Empirical Standard Error S_B^2 of the Buckling

From the measurement of the axial rate distribution the buckling B^2 is derived using the least square fit. In this chapter the uncertainty of B^2 is discussed. The Gaussian theory of error is applied, therefore, the following treatment is restricted to statistical errors only.

The n values y_i with weights g_i and abscissa x_i are measured. The two parameters A, B of the function

$$\xi = A \cos B x \tag{1}$$

are determined by minimizing

$$Q = \sum_{i=1}^{n} g_i (y_i - \xi_i)^2 . \tag{2}$$

To calculate the standard errors S_A, S_B of A, B the linear estimation

$$\begin{aligned} A &= A^o + u \\ B &= B^o + v \end{aligned} \tag{3}$$

is made. The A^o, B^o are estimated values. Then

$$\begin{aligned} S_A &= S_u \\ S_B &= S_v \end{aligned} \tag{4}$$

follows. It is assumed that Eq.(1) can be approximated by

$$\xi_i = \xi_i^o + a_i u + b_i v \tag{5}$$

for sufficiently small u, v.

The coefficients a_i, b_i can be chosen as the partial derivatives of ξ_i at the estimated value.

$$\begin{aligned} a_i &= \left(\frac{\partial \xi_i}{\partial A} \right)^o = \cos B^o x_i = \frac{\xi_i^o}{A^o} \\ b_i &= \left(\frac{\partial \xi_i}{\partial B} \right)^o = - A^o x_i \sin B^o x_i = - x_i \sqrt{A^{o2} - \xi_i^{o2}} . \end{aligned} \tag{6}$$

The sum of squares (Eq.(2)) can be rewritten with (5):

$$Q = \sum_{i=1}^{n} g_i (x_i - \xi_i^o - a_i u - b_i v)^2 \quad . \tag{7}$$

u and v are determined by minimizing (7). Then Eq.(8) holds

$$\begin{aligned} \Sigma g_i a_i a_i \cdot u + \Sigma g_i a_i b_i \cdot v &= \Sigma g_i a_i (y_i - \xi_i^o) \\ \Sigma g_i b_i a_i \cdot u + \Sigma g_i b_i b_i \cdot v &= \Sigma g_i b_i (y_i - \xi_i^o) \quad . \end{aligned} \tag{8}$$

The solutions u, v are in this case linearly independent, that means u, v are estimable. The reverse transformation of (8) yields:

$$\begin{aligned} u &= \frac{\Sigma g_i b_i b_i}{D} \cdot \Sigma g_i a_i (y_i - \xi_i^o) - \frac{\Sigma g_i a_i b_i}{D} \Sigma g_i b_i (y_i - \xi_i^o) \\ v &= \frac{\Sigma g_i a_i b_i}{D} \cdot \Sigma g_i a_i (y_i - \xi_i^o) + \frac{\Sigma g_i a_i a_i}{D} \Sigma g_i b_i (y_i - \xi_i^o) \\ D &= \Sigma g_i a_i a_i \Sigma g_i b_i b_i - (\Sigma g_i a_i b_i)^2 \quad . \end{aligned} \tag{9}$$

According to (3) the estimated variances of A, B are equal to the variances of u, v, respectively. The estimated variances of $(y_i - \xi_i^o)^2$ may be s_i^{o2}. Because the weights g_i are inversely proportional to s_i^2 we set

$$s_i^2 = \frac{1}{g_i} s^2 \quad . \tag{10}$$

Therefore, it follows for s_u^2, s_v^2:

$$\begin{aligned} s_u^2 &= \Sigma g_i \left(\frac{\Sigma g_i b_i b_i}{D} a_i - \frac{\Sigma g_i a_i b_i}{D} b_i \right)^2 s^2 \\ s_v^2 &= \Sigma g_i \left(- \frac{\Sigma g_i a_i b_i}{D} a_i + \frac{\Sigma g_i a_i a_i}{D} b_i \right)^2 s^2 \end{aligned} \tag{11}$$

From Eq.(11) we get:

$$\begin{aligned} s_u^2 &= \frac{\Sigma g_i b_i b_i}{D} s^2 \\ s_v^2 &= \frac{\Sigma g_i a_i a_i}{D} s^2 \quad . \end{aligned} \tag{12}$$

s^2 can be obtained as *

$$s^2 = \frac{Q}{n - \nu} \quad , \tag{13}$$

where ν is the number of degrees of freedom. Finally, we get with (6) for s_A^2, s_B^2 Eq.(12):

$$s_A^2 = \frac{\sum_1^n g_i x_i^2 (A^{o2} - \xi_i^{o2})}{D} \cdot \frac{Q}{n - 2}$$

$$s_B^2 = \frac{\sum_1^n g_i \xi_i^{o2} A^{o-2}}{D} \cdot \frac{Q}{n - 2}$$

$$D = \sum_1^n g_i \xi_i^{o2} A^{o-2} \sum g_i x_i^2 (A^{o2} - \xi_i^{o2}) - \left[\sum_1^n g_i \xi_i^{o} x_i \sqrt{1 - \xi_i^{o2} A^{o-2}}\right]^2 . \tag{14}$$

* Van der Waerden, Mathematische Statistik, Springer Verlag, 1957.

B. Error Estimation of Integrated Rates

To determine the total reaction rates of the core and blanket in slab geometry the measured rates were connected by a smoothed curve and integrated graphically. The accuracy of integration is about 0.25 % in the core and 1% in the blanket determined by repetition. In addition to that error, an uncertainty arises from the accuracy of each measured point. To take this into account the following assumption was made. The integral over the rate distribution along the z-axis can be written as:

$$I = \sum_{i=1}^{n} \delta z_i \cdot R(z_i) \quad . \tag{15}$$

With the error propagation law it is assumed that the error of the integral due to errors in $R(z_i)$ is:

$$(\Delta I)^2 = \sum_{i=1}^{n} \left[\delta z_i \cdot \Delta R(z_i) \right]^2 \tag{16a}$$

$$= \sum_{i=1}^{n} \left[\delta z_i \cdot \frac{\Delta R(z_i)}{R(z_i)} \cdot R(z_i) \right]^2 \quad . \tag{16b}$$

For constant δz_i and $\Delta R(z_i) = \Delta R_{max}$ formula (16a) yields:

$$\frac{\Delta I_{abs}}{I} = \frac{1}{\sqrt{n}} \cdot \frac{\Delta R_{max}}{\bar{R}} \quad , \tag{17a}$$

where n is the number of measured points distributed equidistant over the integration distance and $\bar{R}$ is the average reaction rate. Eq.(16b) yields for constant relative errors $\Delta R(z_i) / R(z_i) = \Delta R_{max}/R_{max}$:

$$\frac{\Delta I_{rel}}{I} = \frac{1}{\sqrt{n}} \cdot \frac{\sqrt{\overline{R^2}}}{\bar{R}} \cdot \frac{\Delta R_{max}}{R_{max}} \quad . \tag{17b}$$

$\frac{\Delta I_{rel}}{I} < \frac{\Delta I_{abs}}{I}$, because $\sqrt{\overline{R^2}} < R_{max}$, therefore, reasonable errors were obtained by application of Eq.(17a).

References

/1/ SEUFERT, H. and D. STEGEMANN: A Method for Absolute Determination of ^{238}U Capture Rates in Fast Zero-Power Reactors. Nucl. Sci. Eng. 28, 277 (1967).

/2/ SCHRÖDER, R. et al.: Physics Investigation of Uranium-Fueled Fast Steam-Cooled Reactors in SNEAK, Assemblies 3A-0, 3A-2, and 3A-3. To be published.

/3/ WINTZER, D.: Heterogeneity Calculations Including Space Dependent Resonance Self-Shielding. IAEA-Symposium on Fast Reactor Physics and Related Safety Problems, SM-101/13, Karlsruhe, 1967.

/4/ BLANK, K.H. and H. SEUFERT: An Automatic Sample Changer with a Special Changing Method for γ- and γ-γ-Active Sources. Nucl. Instr. Meth. 46, 86 (1967).

/5/ MICHAELIS, W., H. SCHMIDT, and C. WEITKAMP: Die Zählratenabhängigkeit des Verstärkungsfaktors und des Auflösungsvermögens bei Photomultipliern vom Typ RCA 6810 A. Nucl. Instr. Meth. 21, 65 (1963).

/6/ ABAGJAN, L.P., N.O. BAZAZJANC, I.I. BONDARENKO, and M.N. NIKOLAEV: Gruppenkonstanten schneller und intermediärer Neutronen für die Berechnung von Kernreaktoren. KFK-tr-144, Translation, 1963.

/7/ KÜSTERS, H. et al.: The Group Cross-Section Set KFK-SNEAK. Preparation and Results. IAEA-Symposium on Fast Reactor Physics and Related Safety Problems, SM-101/12, Karlsruhe, 1967.

/8/ PÖNITZ, W.P., D. KOMPE, H.O. MENLOVE, and K.H. BECKURTS. Some New Measurements and Renormalizations of Neutron Capture Cross Section Data in the keV Energy Region. IAEA-Symposium on Fast Reactor Physics and Related Safety Problems, SM-101/9, Karlsruhe, 1967.

/9/ STEGEMANN, D. et al.: Physics Investigations of a 670 l Steam Cooled Fast Reactor System in SNEAK, Assembly 3A-1. IAEA-Symposium on Fast Reactor Physics and Related Safety Problems, SM-101/11, Karlsruhe, 1967.

/10/ ARNOLD, M.J., W.N. FOX, C.F. GEORGE, and R. RICHMOND: Variation of k-inf with Coolant Density for a Plutonium Fueled Steam-Cooled Fast Reactor Lattice. IAEA-Symposium on Fast Reactor Physics and Related Safety Problems, SM-101/43, Karlsruhe, 1967.

Squared relative errors / Source	R_f^{25}	R_f^{28}	R_c^{28}	$\frac{R_f^{28}}{R_f^{25}}$	$\frac{R_c^{28}}{R_f^{25}}$
Statistics and isotopic composition	$2x1 \cdot 10^{-6}$	$2x25 \cdot 10^{-6}$	$9 \cdot 10^{-6}$	$52 \cdot 10^{-6}$	$11 \cdot 10^{-6}$
Half-live of ^{239}Np and positioning	-	-	$2.50 \cdot 10^{-4}$	-	$2.25 \cdot 10^{-4}$
Calibration	$4 \cdot 10^{-4}$	$4 \cdot 10^{-4}$	$25 \cdot 10^{-6}$	$8 \cdot 10^{-4}$	$4.25 \cdot 10^{-4}$
Flux monitoring	$1 \cdot 10^{-4}$	$1 \cdot 10^{-4}$	-	-	$1 \cdot 10^{-4}$
Stabilization	$2x25 \cdot 10^{-6}$	$2x25 \cdot 10^{-6}$	-	$1 \cdot 10^{-4}$	$50 \cdot 10^{-6}$
Total	$5.52 \cdot 10^{-4}$	$7 \cdot 10^{-4}$	$2.84 \cdot 10^{-4}$	$9.52 \cdot 10^{-4}$	$8.11 \cdot 10^{-4}$
% error	2.4	2.7	1.7	3.0	2.9

Tab.1 Errors in Reaction Rates and Reaction Rate Ratios

	Al	C	Co	Cr	Fe	H	Mg	Mn	Ni	O	Si	Ti	^{235}U	^{238}U	Mo + Nb
Central core zone	129.1	9.32	.19	34.53	121.9	17.92	.64	1.94	18.54	145.3	1.88	.4	20.31	81.04	.39
Blanket	-	.14	-	11.08	40.4	-	-	-	98.4	-	.46	.01	1.63	399.4	-

Tab.2 Atomic Densities in $10^{20}/cm^3$

Material / Platelet	Al(+Mg)	C	Cr(+Mn)	Fe(+Co)	H	Mo	Ni	O	Si	Ti	^{238}U	^{235}U
U 20%	-	-	11.7	38.92	-	-	12.72	-	-	-	324.2	81.24
Al_2O_3	387.7	-	11.7	38.92	-	-	5.67	581.1	-	-	-	-
SS + CH_2	-	37.31	110.1	371.7	71.68	1.58	50.11	-	6.45	1.63	-	-
Al 25%	131.2	-	12.2	38.92	-	-	5.67	-	1.08	-	-	-

Tab.3 Atomic Densities in $10^{20}/cm^3$ in the Unit Cell

	Experiment	SNEAK set homogeneous	PMB set homogeneous	ABN set homogeneous	Heterogeneity correction for SNEAK set
$\frac{\sigma_f^{28}}{\sigma_f^{25}}$	0.0338±0.0010	0.0297	0.0295	0.0301	- 1.5 %
$\frac{\sigma_c^{28}}{\sigma_f^{25}}$	0.130 ±0.004	0.137	0.136	0.122	- 1.8 %
k_{eff}	1.	0.984	0.980	1.004	

Tab.4 Central Reaction Rate Ratios

	Experiment	SNEAK set heterogeneous	SNEAK set homogeneous	ABN set homogeneous
R_f^{25}	8.03 ± 0.03	8.40	8.47	8.25
R_f^{28}	8.92 ± 0.03	9.16	9.30	9.04
R_c^{28}	7.87 ± 0.03	8.28	8.35	8.18

Tab.5 Experimental and Theoretical Bucklings in $10^{-4}/cm^2$

Integral	Experiment	Theory / Experiment			
		SNEAK set homogeneous	PBM set homogeneous	ABN set homogeneous	SNEAK set heterogeneous
$\varrho^{28} \int_{\text{core}} R_c^{28}(z)\, dz$	$(5.23 \pm 0.10) \cdot 10^8$	1.057	1.048	0.940	1.058
$\varrho^{28} \int_{\text{blanket}} R_c^{28}(z) dz$	$(2.56 \pm 0.06) \cdot 10^8$	0.999	1.003	0.985	1.011
$\varrho^{25} \int_{\text{core}} R_f^{25}(z)\, dz$	$(1.006 \pm 0.023) \cdot 10^9$	1.000	1.000	1.000	1.000
$\varrho^{25} \int_{\text{blanket}} R_f^{25}(z) dz$	$(7.90 \pm 0.20) \cdot 10^6$	1.018	1.022	1.088	1.030
$(1 + \overline{\alpha^{25}})\ \text{IBR}_z$	0.77 ± 0.03	1.039	1.034	0.957	1.042
k_{eff}	1.	0.984	0.980	1.004	0.985

Tab.6 Measured Space Integrated Reaction Rates in $\text{sec}^{-1}\text{cm}^{-2}$ and the Ratio of Theory to Experiment

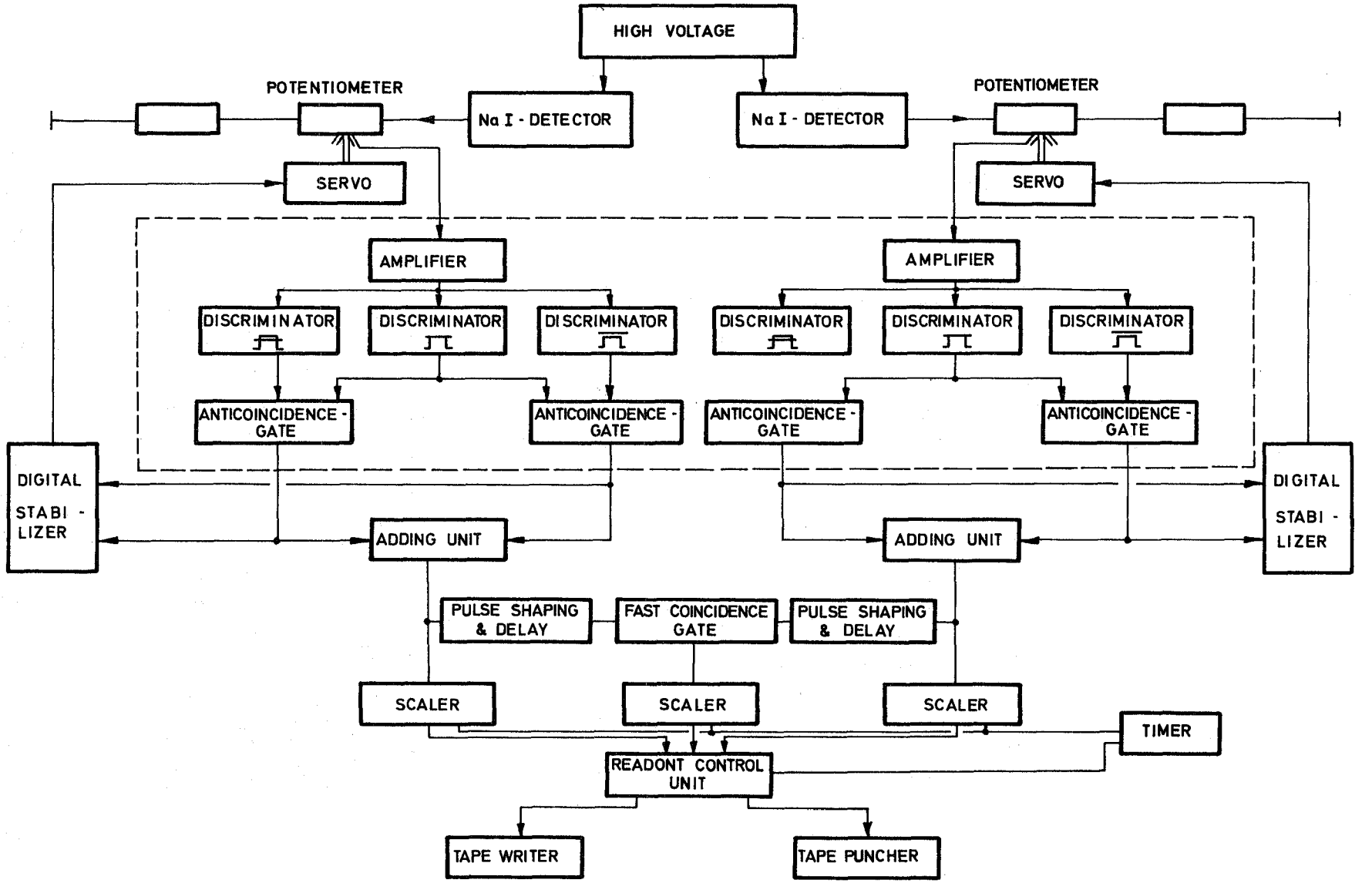

FIG. 1 BLOCK DIAGRAM OF THE γ - X - RAY - COINCIDENCE EQUIPMENT

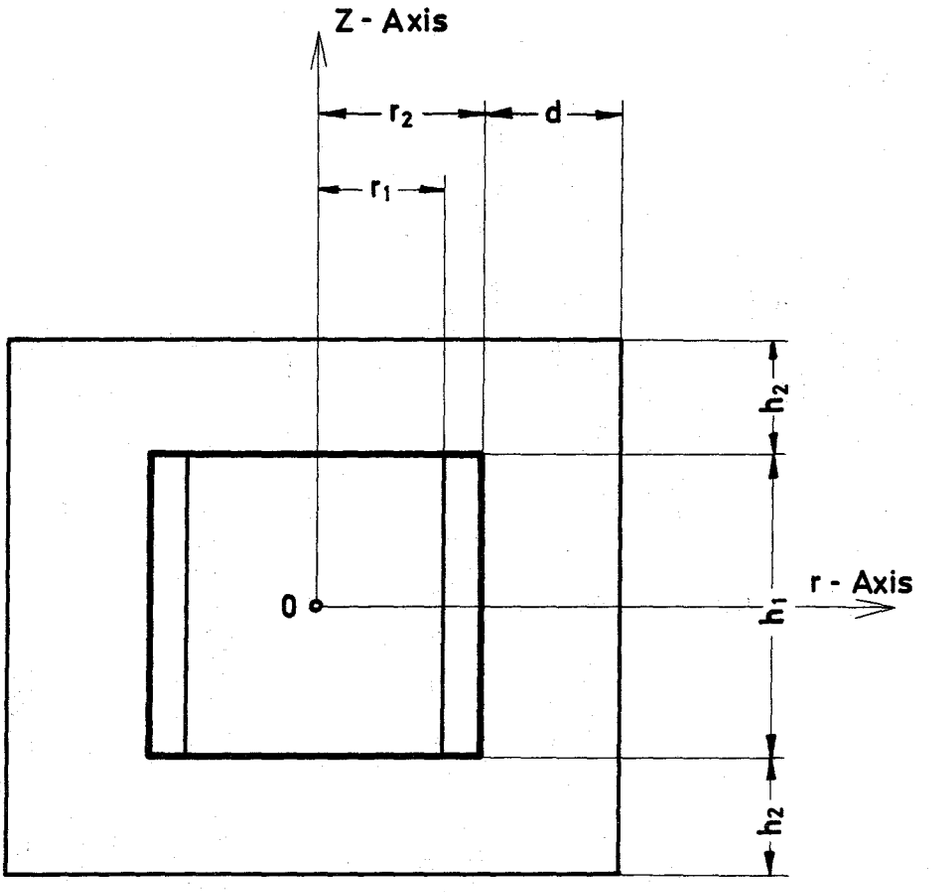

Radius of Core Zone 1	r_1 =	33.76 cm
Radius of Core Zone 2	r_2 =	44.66 cm
Thickness of Radial Blanket	d =	36.2 cm
Height of Core Zone	h_1 =	80.54 cm
Thickness of Axial Blanket	h_2 =	30.5 cm

Fig. 2 Vertical Cross Section through the Cylindrical Reactor SNEAK 3A - 2

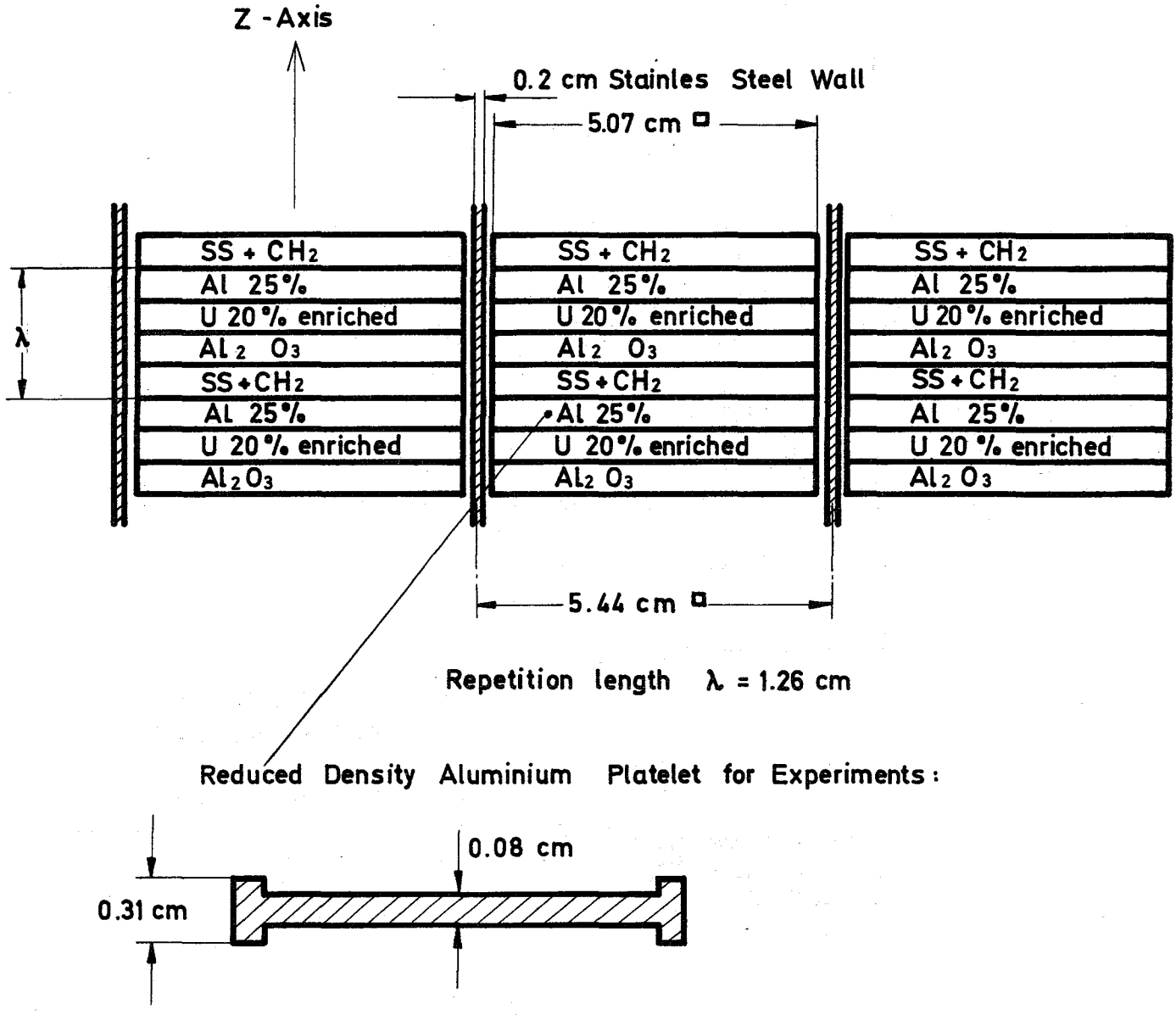

FIG. 3 CELL STRUCTURE OF SNEAK 3A-2

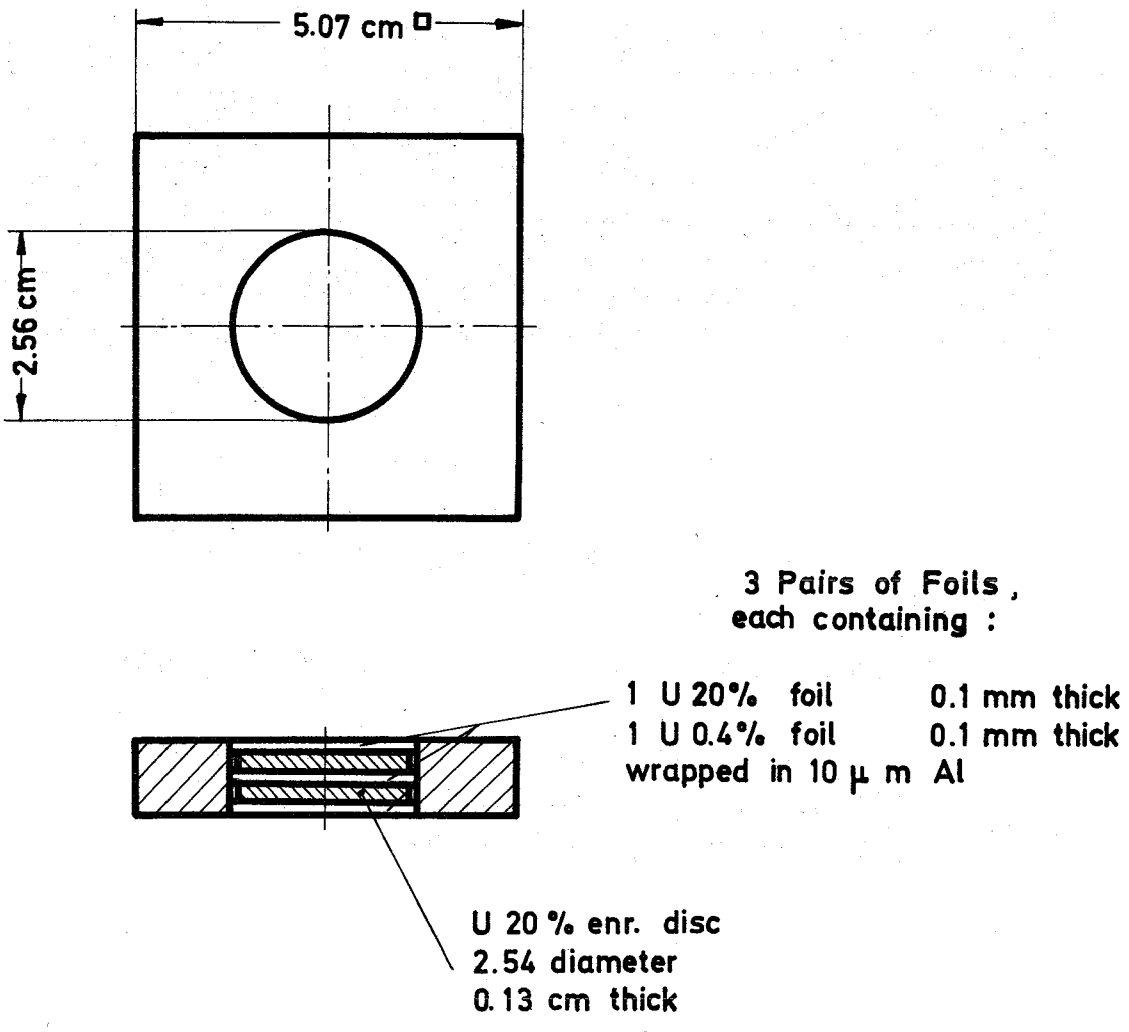

FIG. 4 ENRICHED URANIUM PLATELET USED FOR REACTION RATE MEASUREMENTS

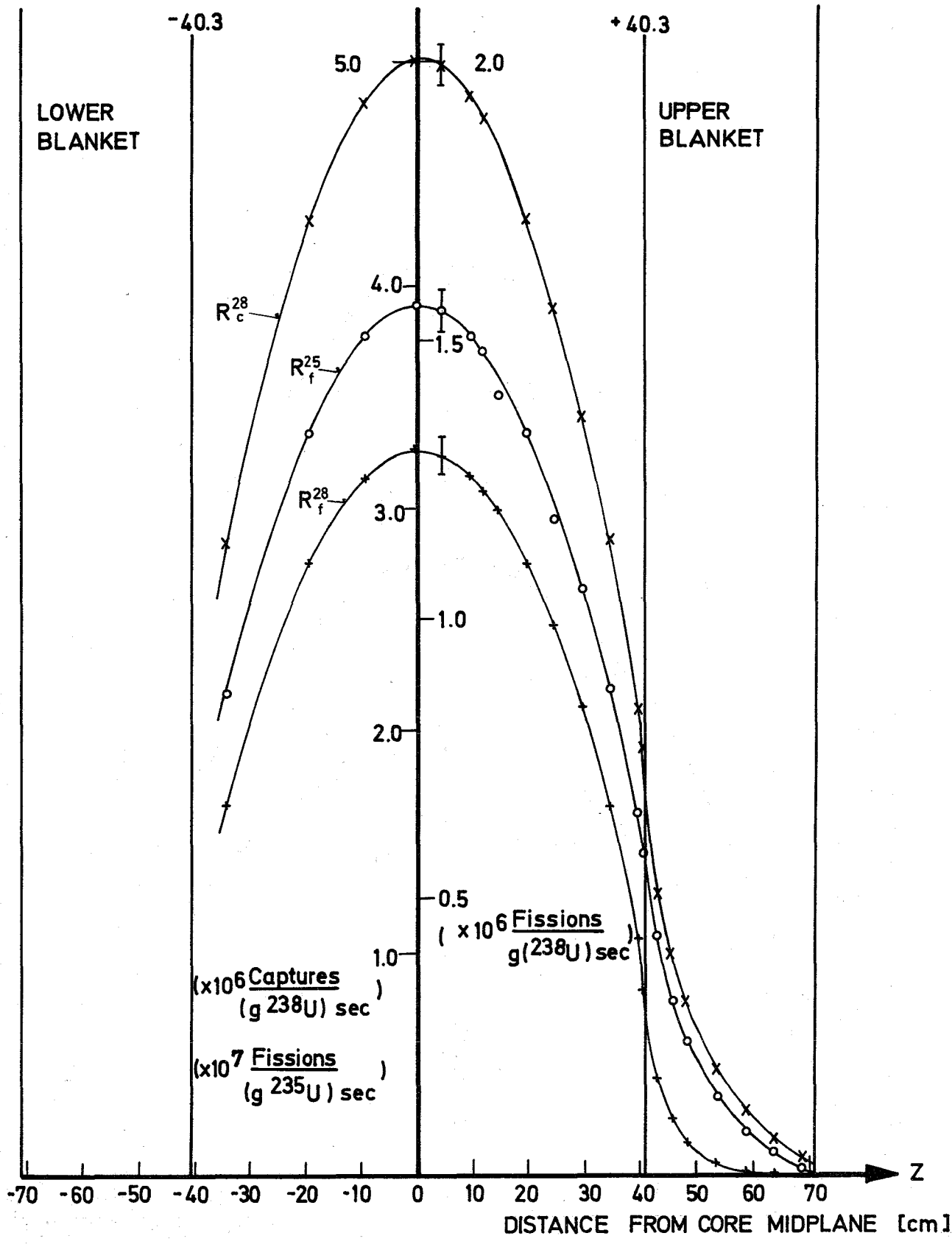

FIG. 5 FISSION AND CAPTURE RATE TRAVERSES ALONG THE AXIS OF SNEAK 3A-2

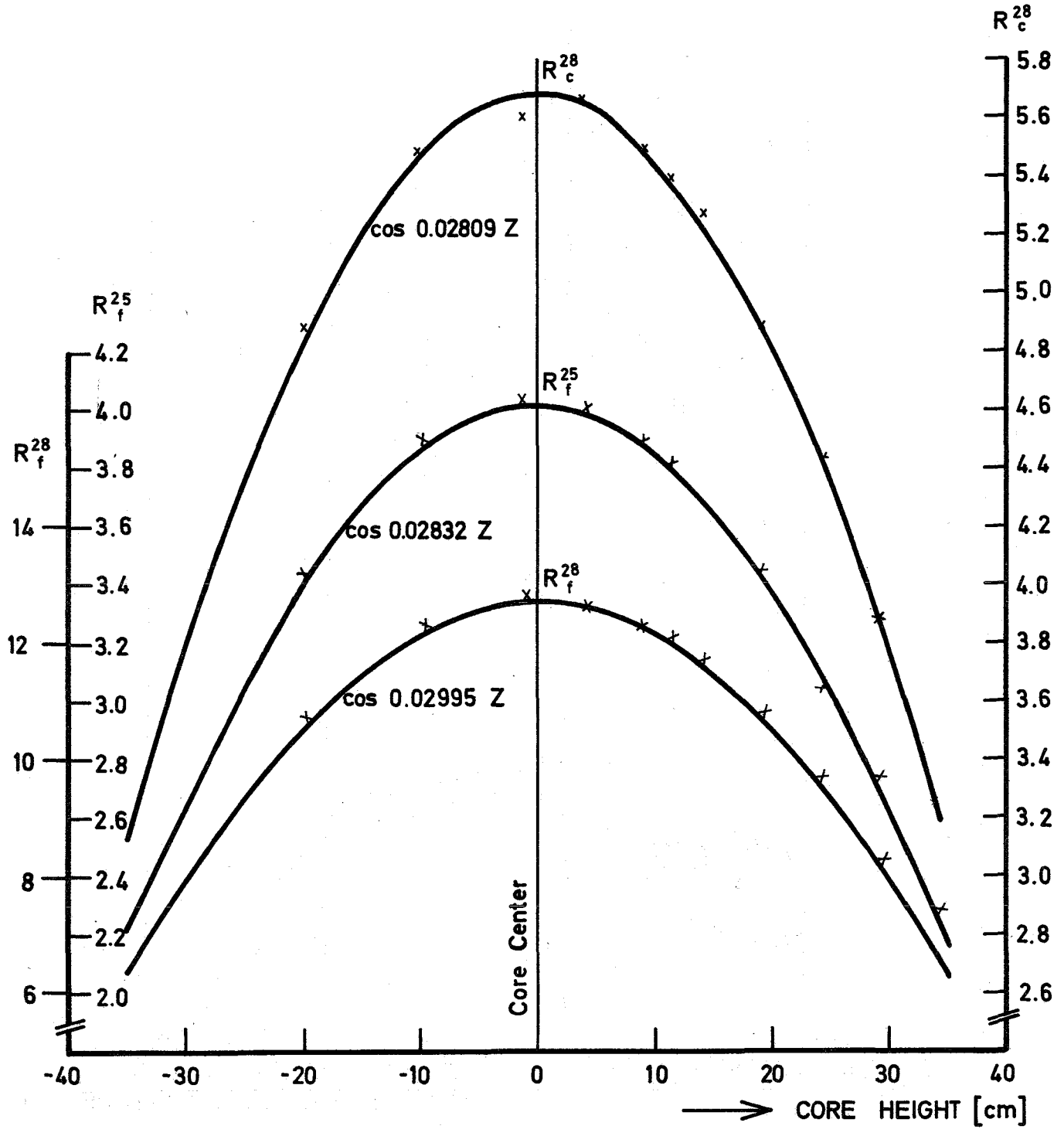

FIG. 6 COSINE - FIT TO MEASURED RATE DISTRIBUTIONS

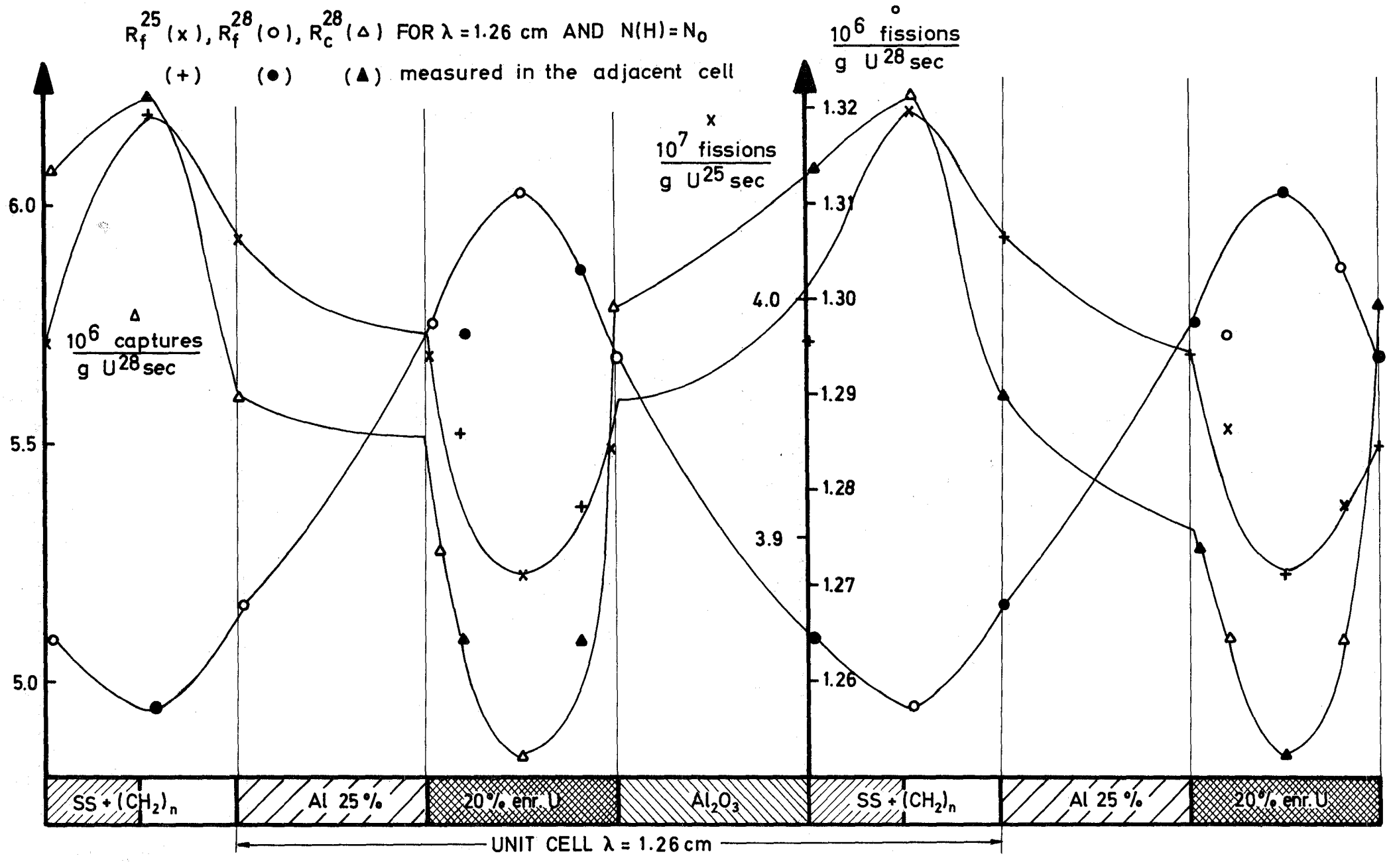

FIG. 7 REACTION RATE DISTRIBUTION IN THE NORMAL CELL

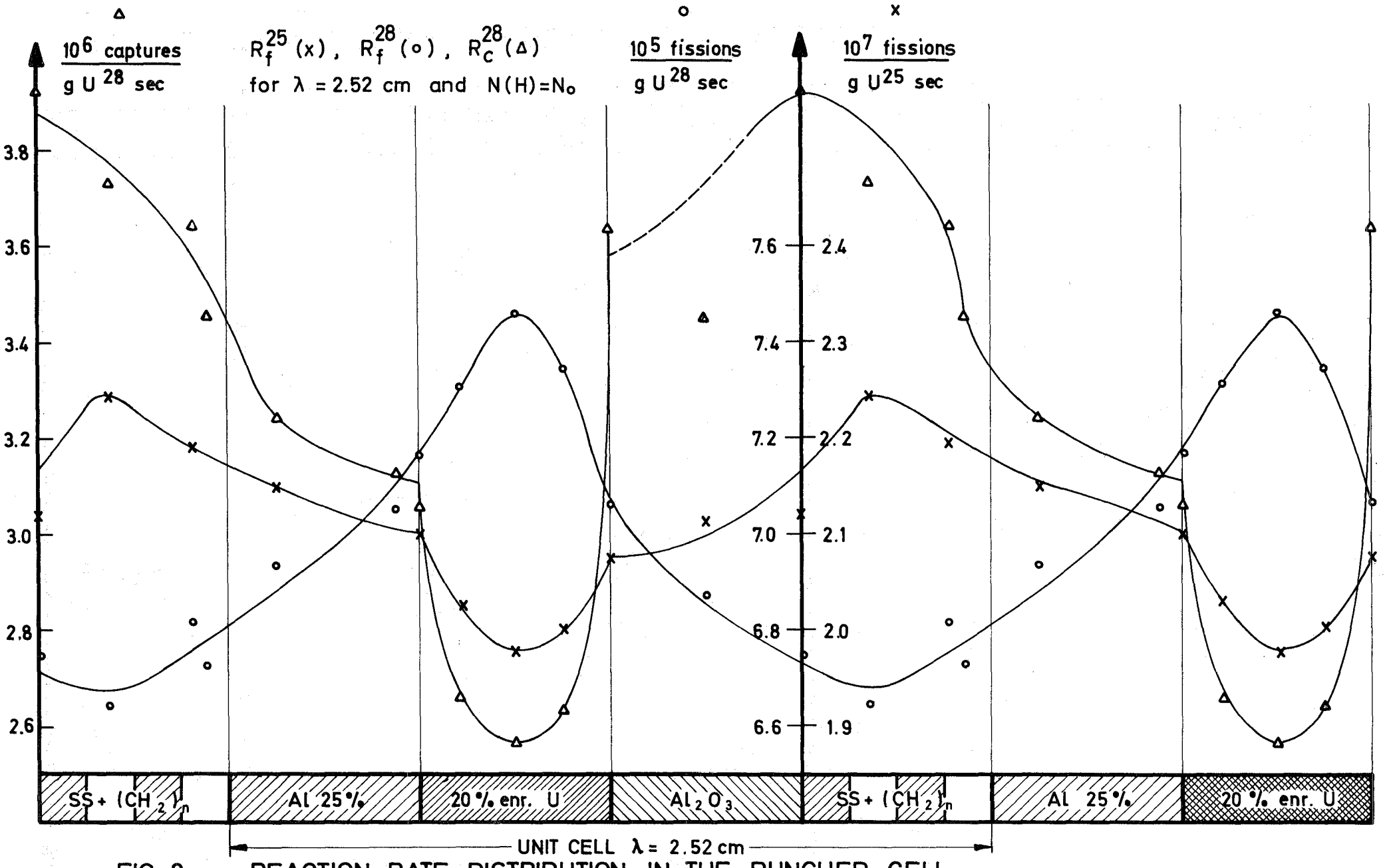

FIG. 8 REACTION RATE DISTRIBUTION IN THE BUNCHED CELL

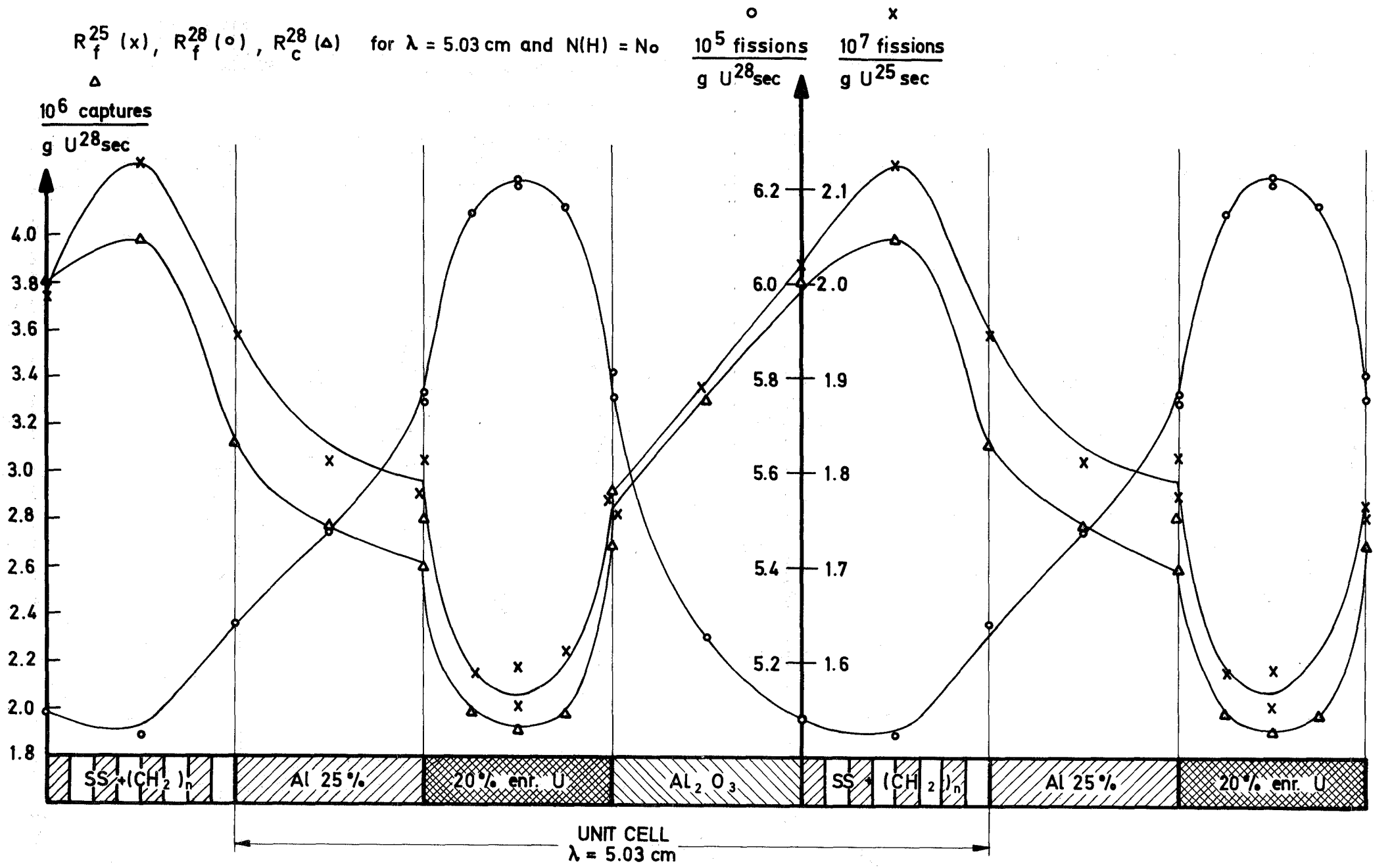

FIG.9 REACTION RATE DISTRIBUTION IN THE DOUBLE BUNCHED CELL

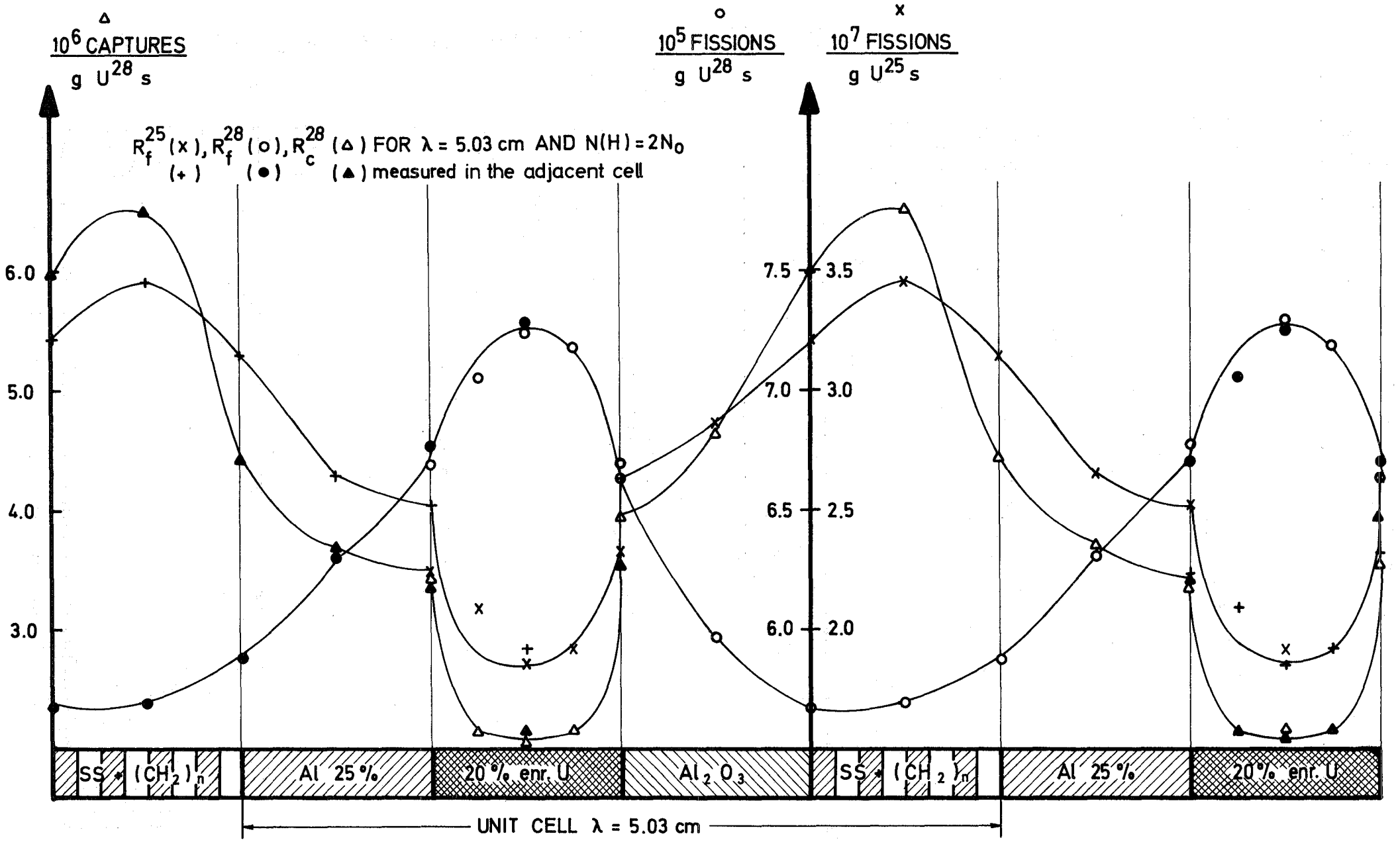

FIG. 10 REACTION RATE DISTRIBUTION IN THE DOUBLE BUNCHED CELL WITH DOUBLE HYDROGEN CONTENT

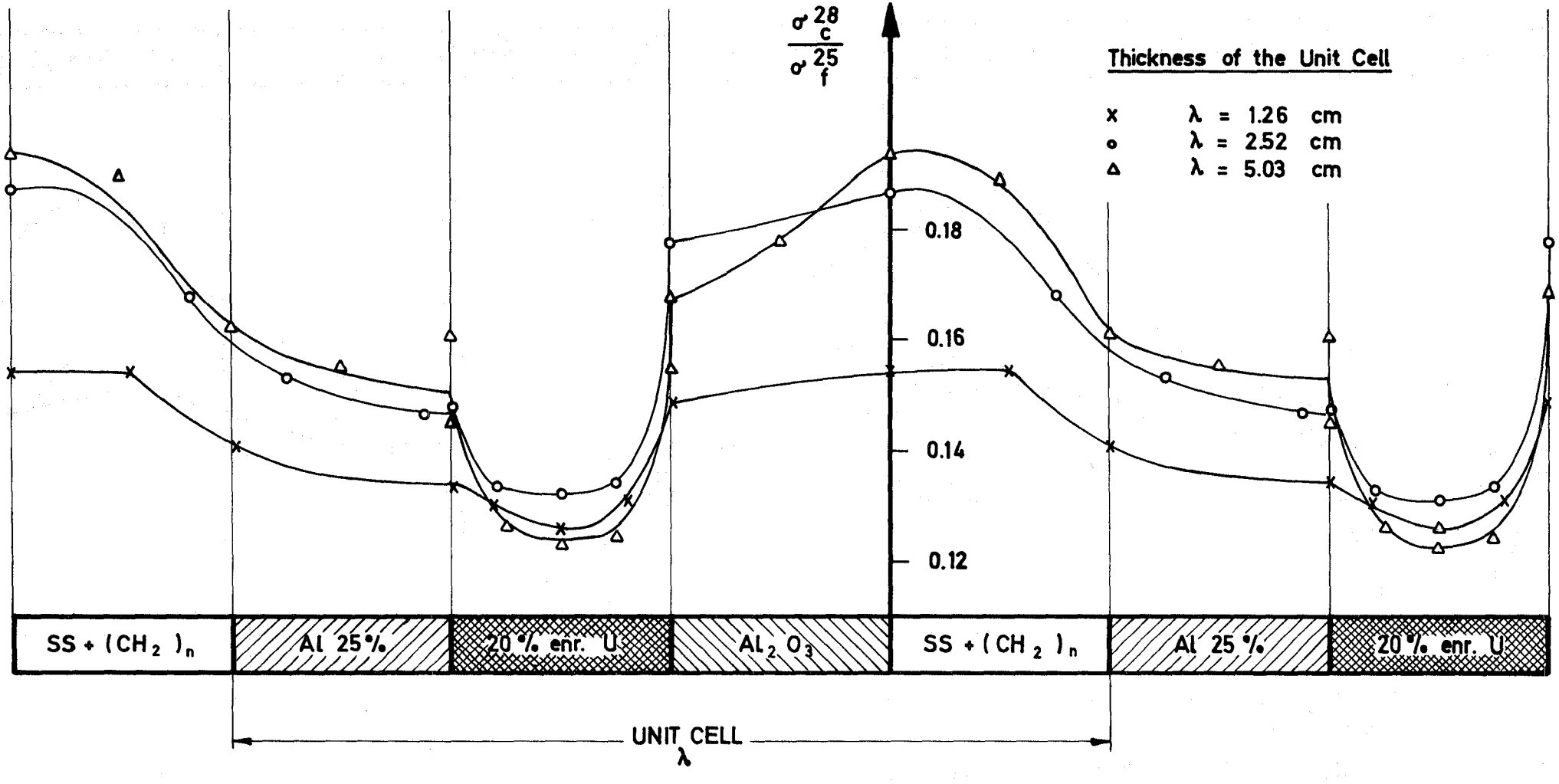

FIG. 11 $\sigma_c^{28} / \sigma_f^{25}$ IN ASSEMBLY 3A-2 FOR THREE DEGREES OF BUNCHING

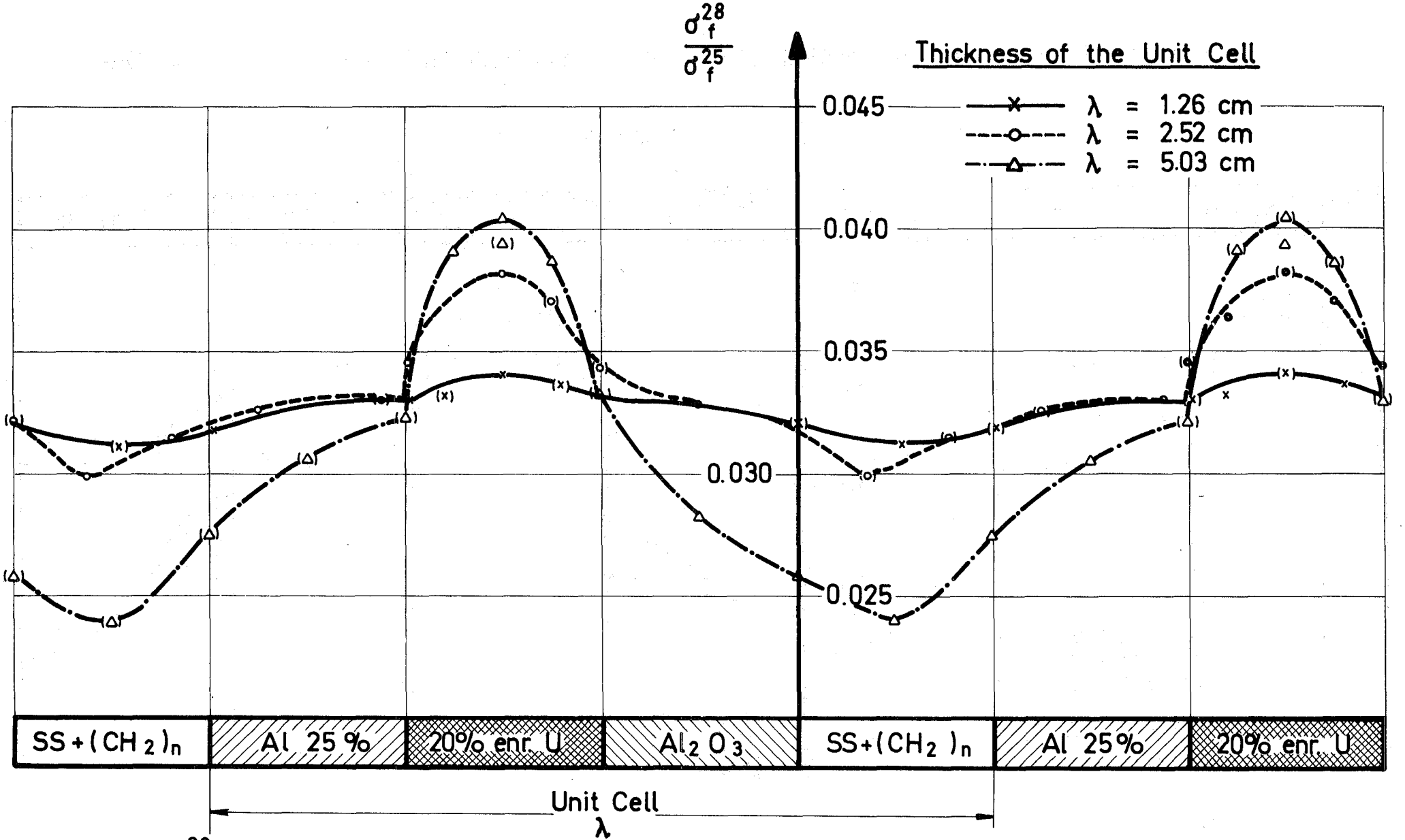

FIG. 12 $\frac{\sigma_f^{28}}{\sigma_f^{25}}$ IN ASSEMBLY 3A-2 FOR THREE DEGREES OF BUNCHING

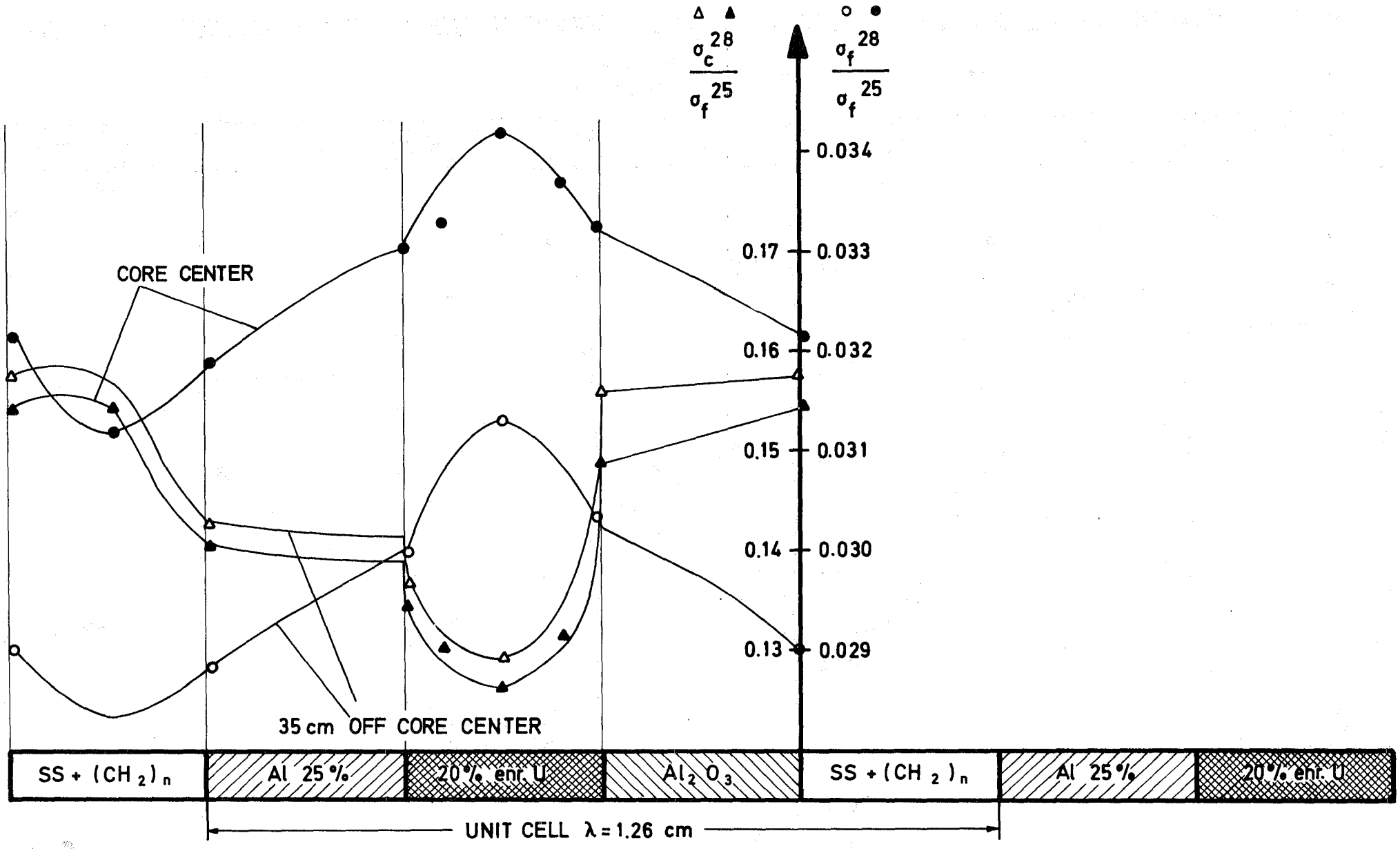

FIG. 13 REACTION RATE RATIOS NEAR THE CORE CENTER AND THE CORE-BLANKET BOUNDARY

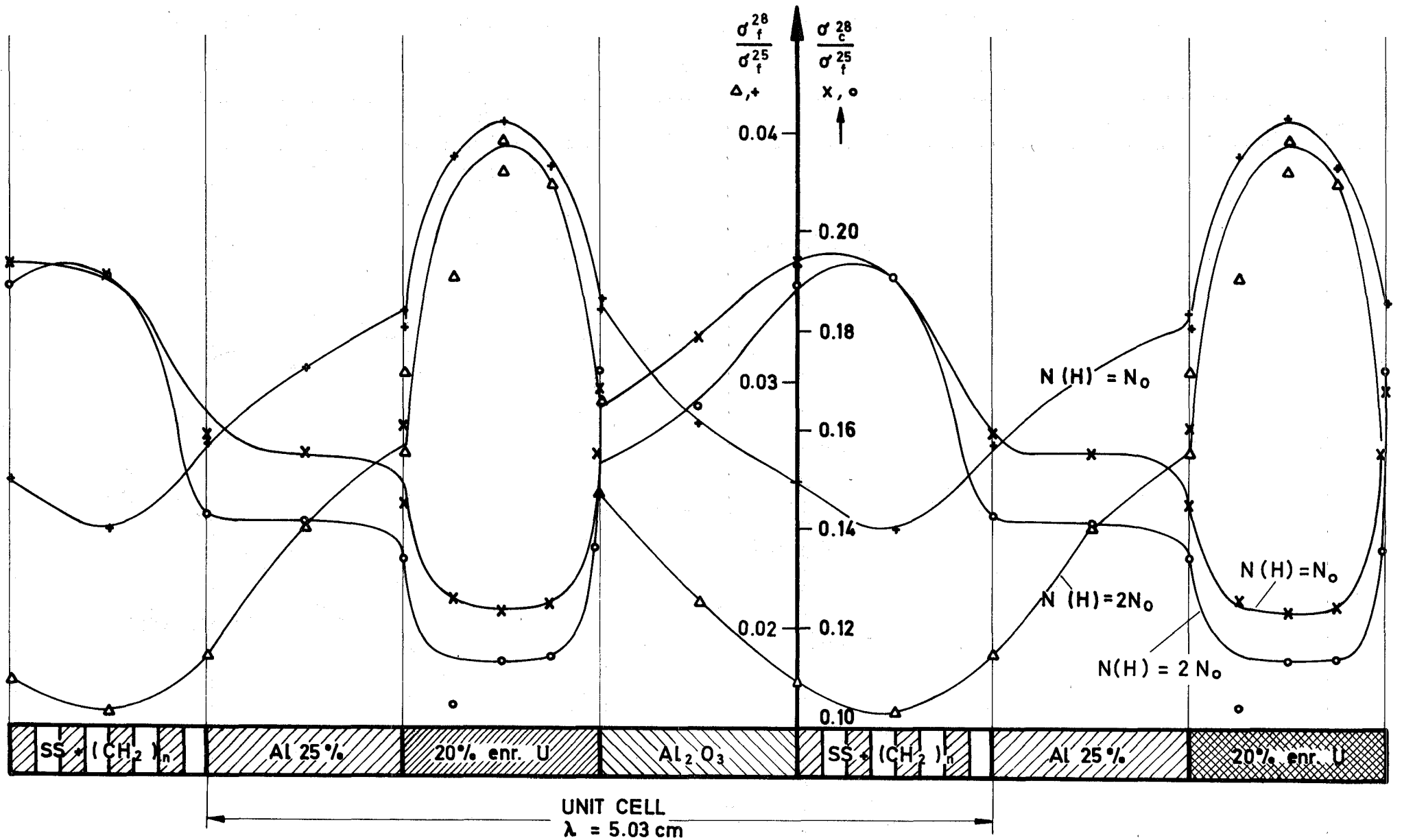

FIG. 14 REACTION RATE RATIOS IN DOUBLE-BUNCHED CELLS WITH DIFFERENT HYDROGEN CONTENT

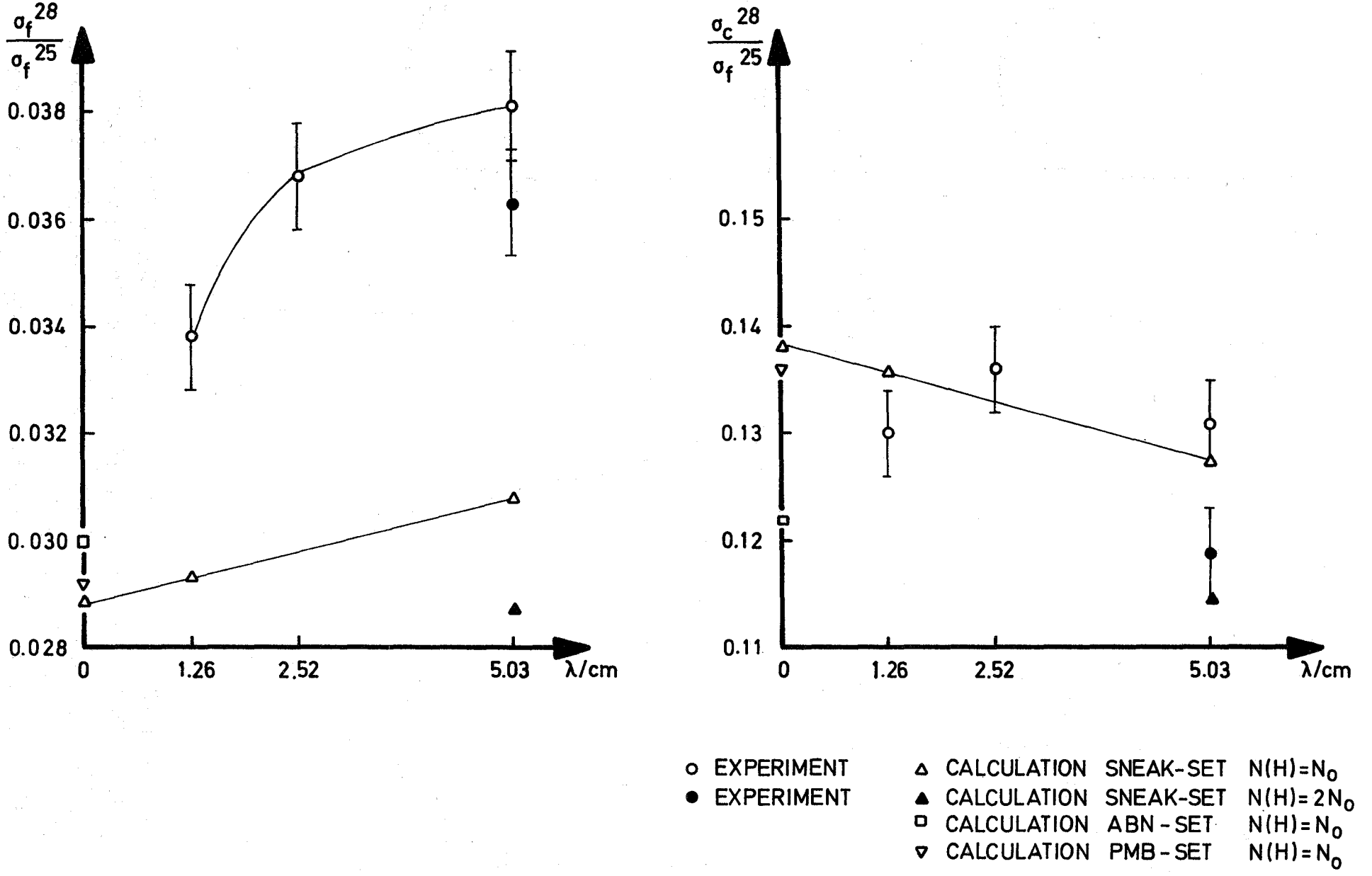

FIG. 15 CENTRAL REACTION RATE RATIOS FOR DIFFERENT DEGREES OF BUNCHING

FIG. 16

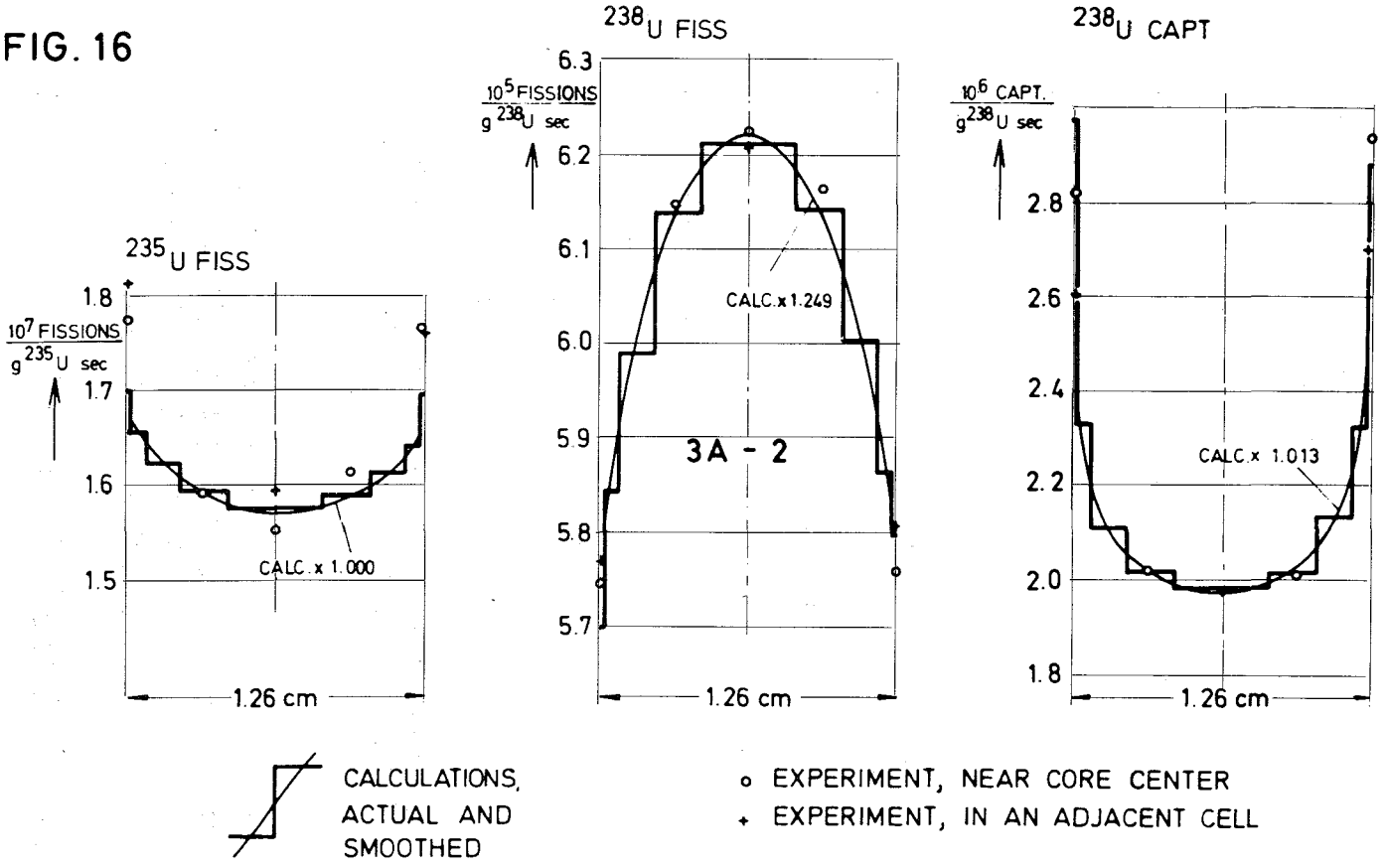

FIG. 17

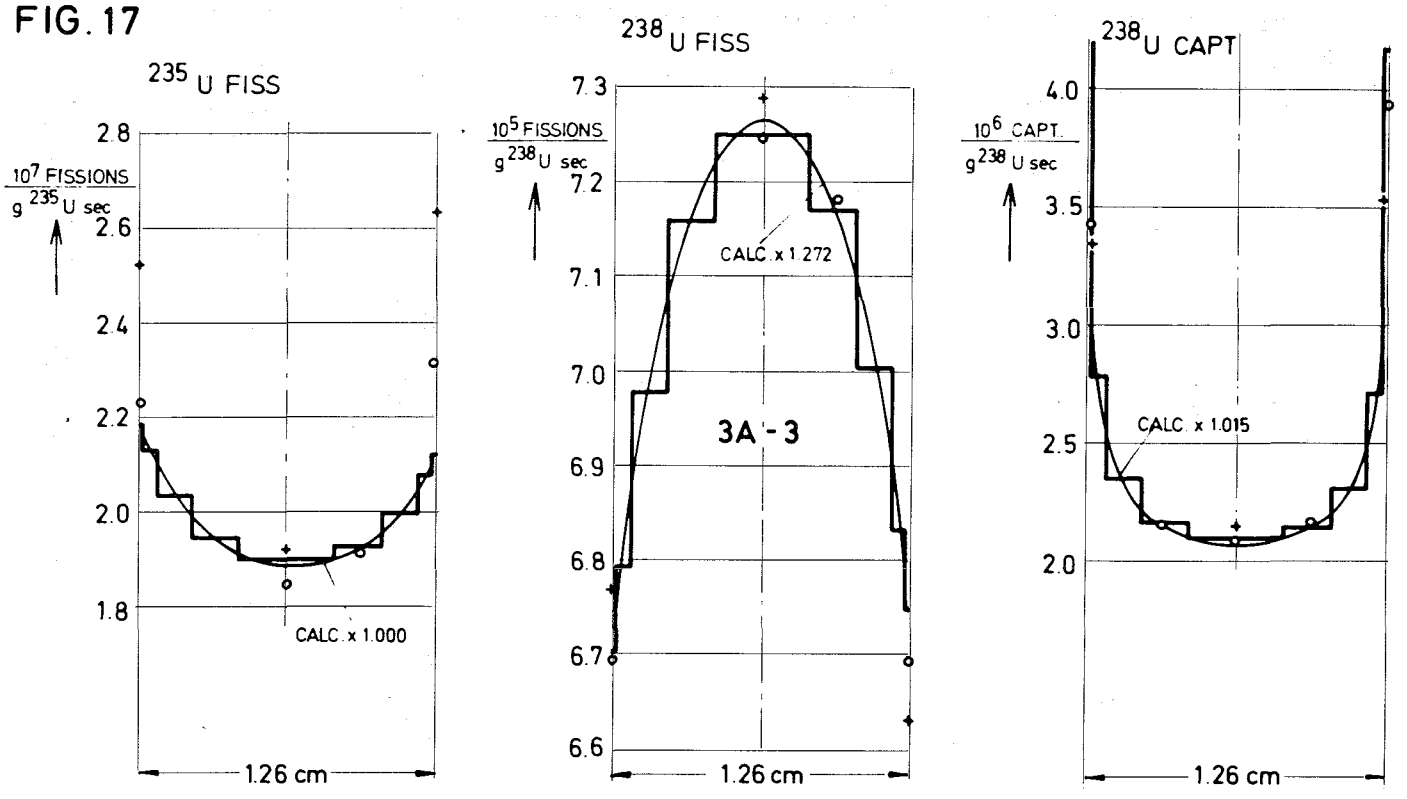

COMPARISON OF EXPERIMENTAL AND CALCULATED LOCAL VARIATION OF REACTION RATES WITHIN THE FUEL ZONE (20% ENRICHED URANIUM) OF SNEAK - ASSEMBLIES 3A-2 (FIG. 16) AND 3A-3 (FIG. 17).
THE CALCULATIONS ARE BASED ON THE SNEAK SET.

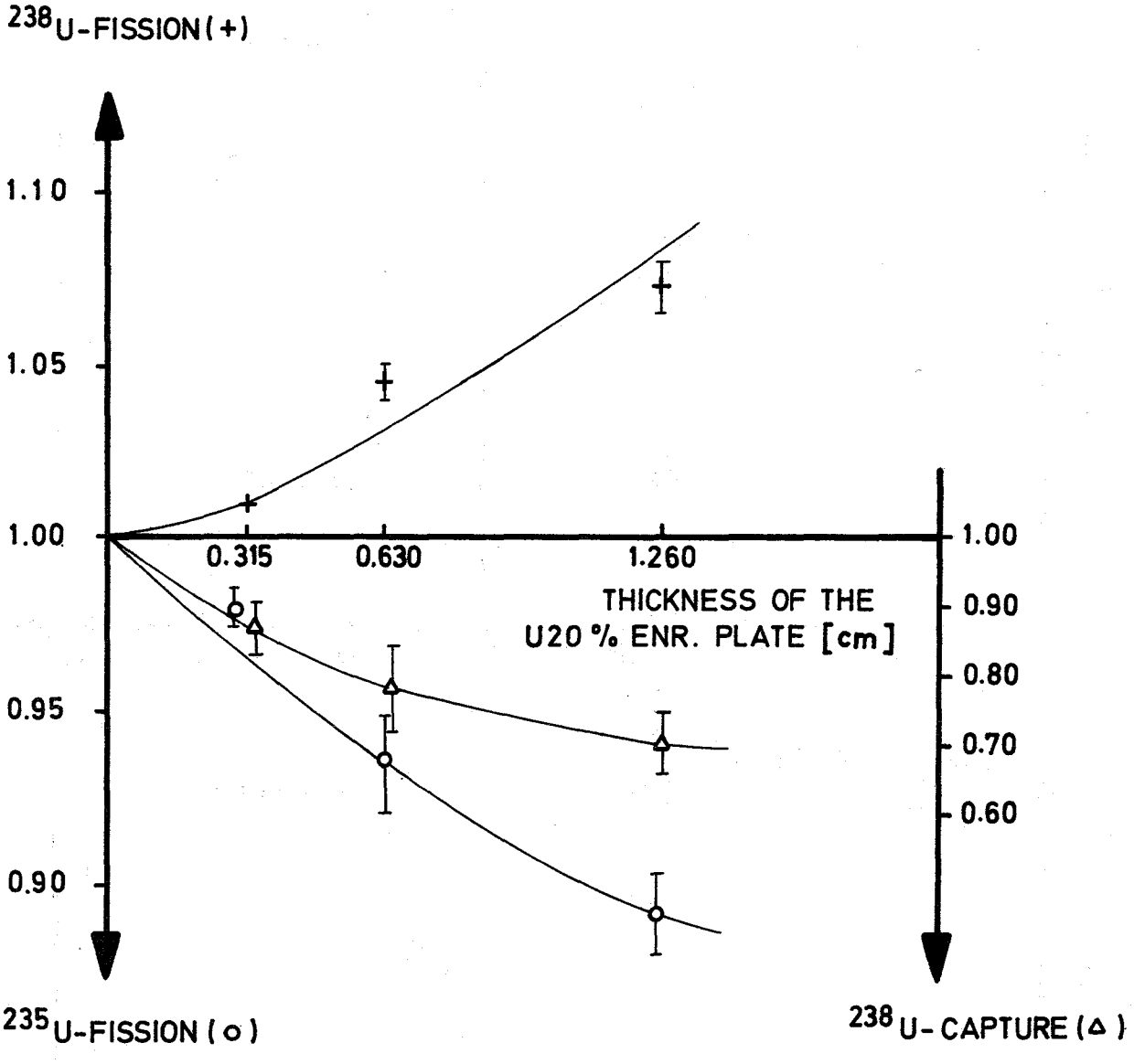

FIG. 18 RATIO OF REACTION RATES IN THE CENTER TO RATES NEAR THE SURFACE OF THE FUEL PLATE FOR DIFFERENT DEGREES OF BUNCHING

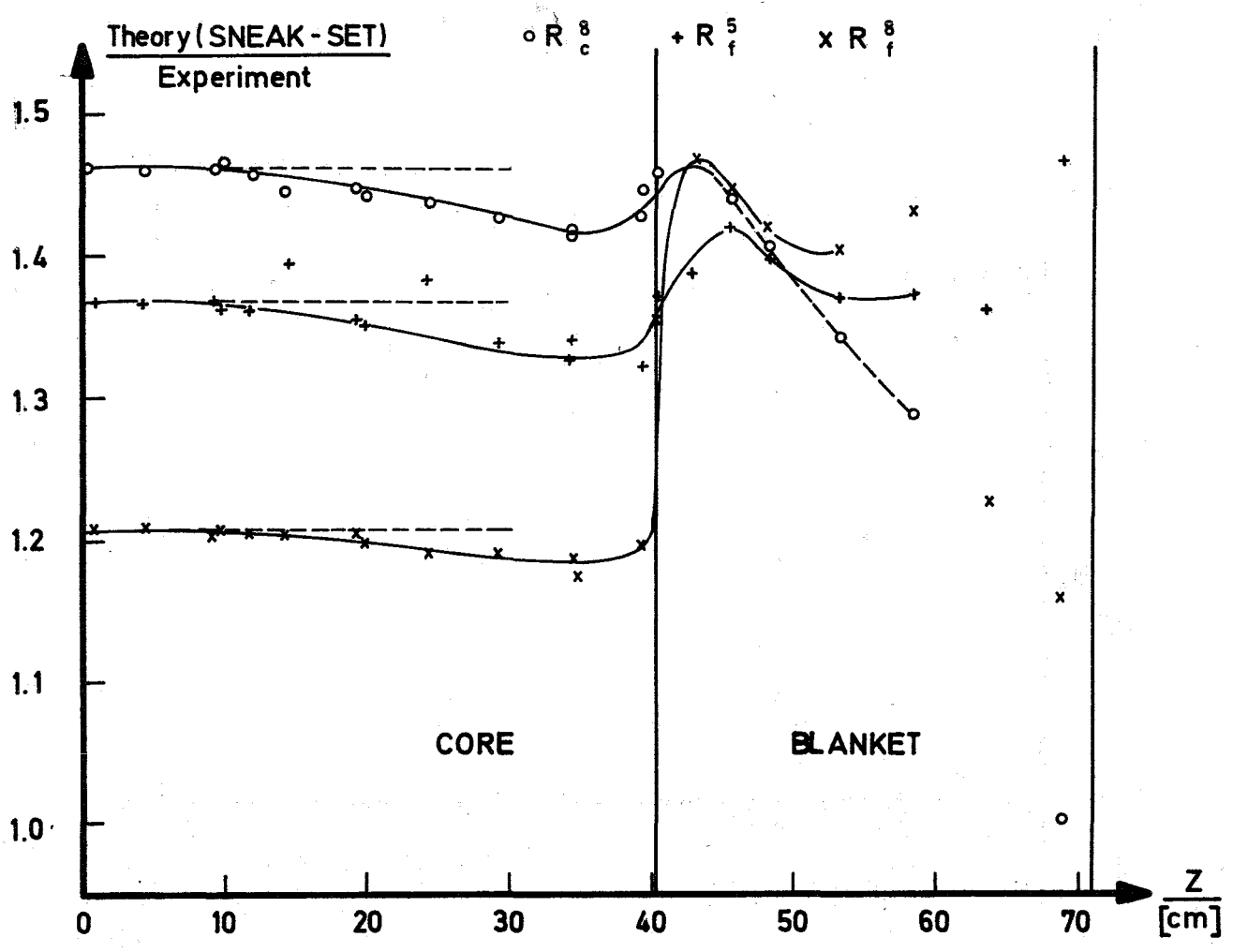

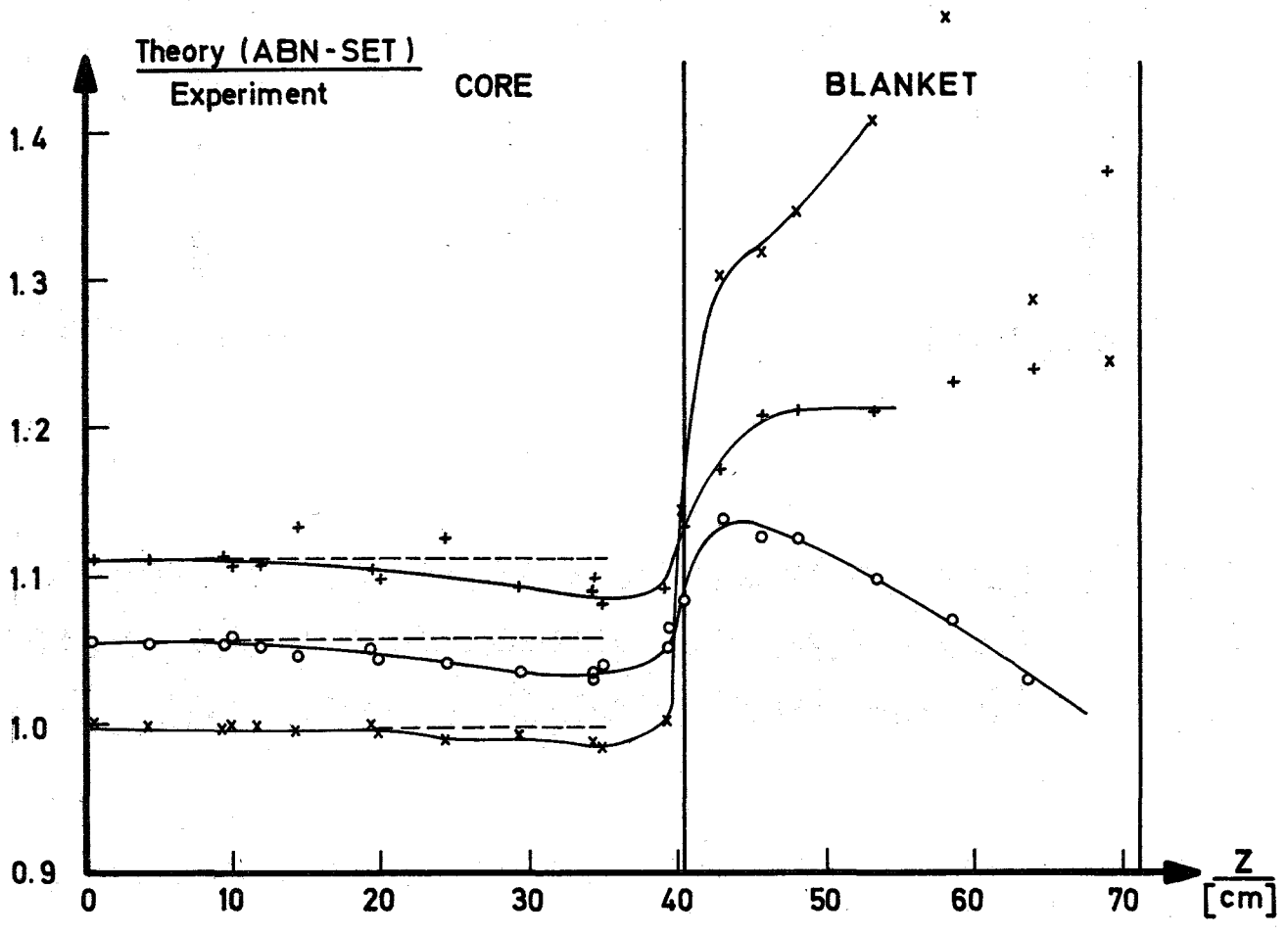

FIG. 19 THE RATIO OF CALCULATED TO MEASURED REACTION RATES ALONG THE CENTRAL REACTOR AXIS

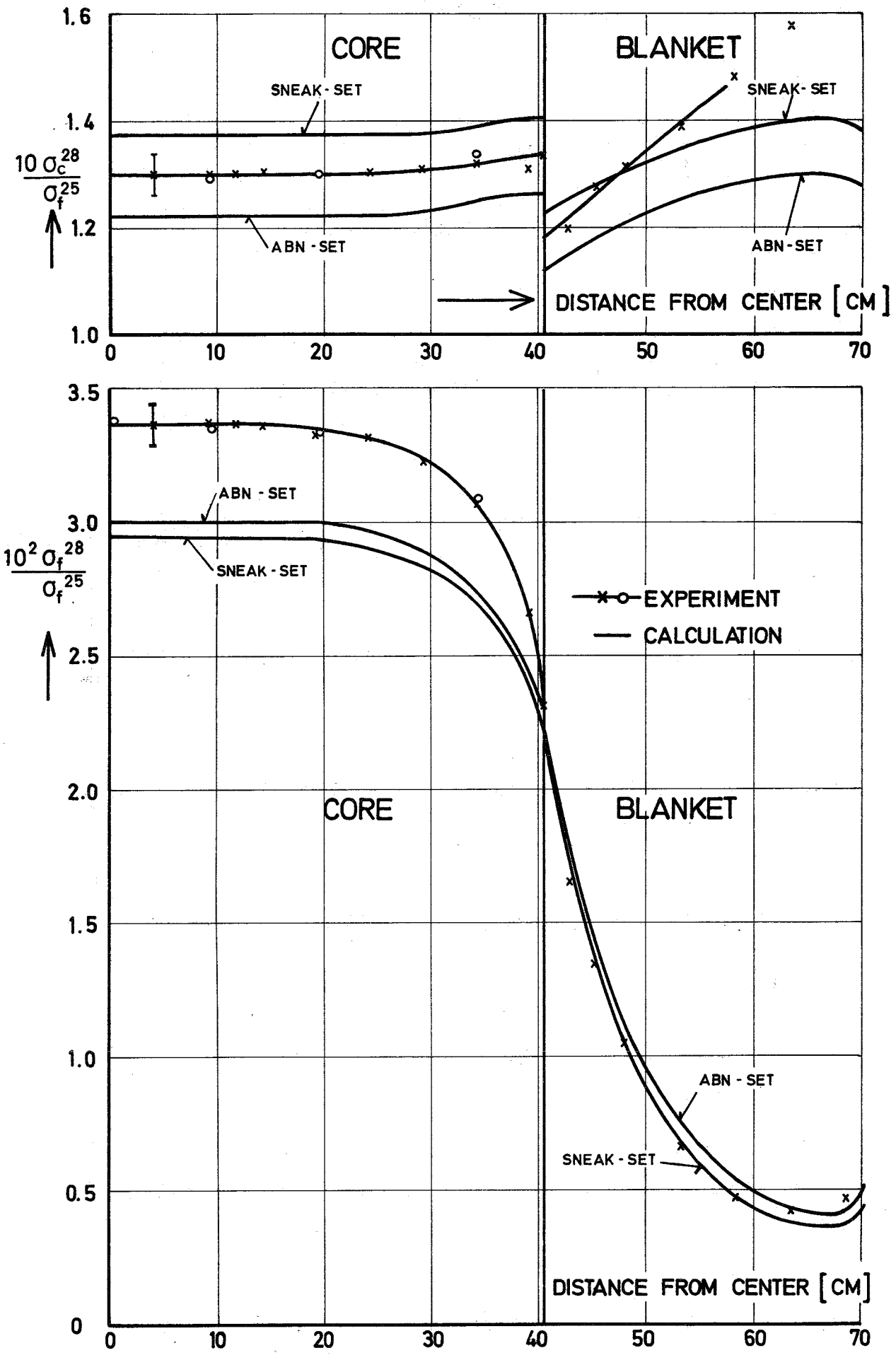

FIG. 20 COMPARISON OF MEASURED AND CALCULATED REACTION RATE RATIOS ALONG THE CORE AXIS IN SNEAK ASSEMBLY 3A-2